POLITECNICO
MILANO 1863

SCUOLA DI INGEGNERIA INDUSTRIALE
E DELL'INFORMAZIONE

Parameterizing a Complete Guitar Model for Vibroacoustic Analysis

Tesi di Laurea Magistrale in
Music and Acoustic Engineering

Author: **Riccardo Di Bella**

Student ID: 101239
Advisor: Prof. Fabio Antonacci
Co-advisors: Sebastian Gonzalez
Academic Year: 2023-24

Abstract

Which geometrical or material features determine the quality of an instrument is probably the most debated matter among guitar makers, but also one that is seldom approached with a scientific mindset. Numerical simulations have proven to be an effective tool for providing rigorous answers to such questions, as they facilitate the testing of multiple models within a shorter time frame, while still providing highly accurate results. However, these approaches are limited by the availability of instrument models which can be adjusted on the fly without excessive effort, possibly even in an automated way. In this perspective, the advantage offered by the use of parametric models, which has recently received particular attention in research, becomes evident.

In this work we develop a parametric and CAD native model of a complete guitar, enabling convenient control over the geometrical features which are considered key in the context of guitar making. In particular, we focus on the parameterization of the outline shape and the soundboard bracing. Additionally, we utilize our new parametric model to conduct a set of simulations based on the Finite Element Method. By doing so, we investigate the effect of some common geometrical variations when these are applied on a full guitar model, including the effect of the surrounding air. The effect is evaluated both by looking at the eigenfrequency variations and at the frequency response of the instrument, in the form of its bridge mobility and radiated sound.

Our findings are both in line with previous studies, proving the validity of our approach, but also present some novel results. In particular, we demonstrate that the uppermost transverse bars of the soundboard do not play any significant role in either shaping the instrument timbre or improving its radiation efficiency. Most importantly, we show how our model can be used to facilitate future research on the physics of guitars.

Keywords: musical acoustics, guitar, parametric modeling, modal analysis, finite element method, frequency response

Abstract in lingua italiana

Quali caratteristiche geometriche o materiali determinino la qualità di uno strumento è forse la questione più dibattuta tra i liutai, ma anche una che raramente viene affrontata con un approccio scientifico. Le simulazioni numeriche si sono dimostrate uno strumento efficace per fornire risposte rigorose a tali domande, in quanto facilitano l'analisi di diversi modelli in breve tempo, pur fornendo risultati altamente accurati. Tuttavia, questi approcci sono limitati dalla disponibilità di modelli geometrici modificabili rapidamente senza eccessivo sforzo, possibilmente anche in maniera automatizzata. In quest'ottica appare quindi evidente il vantaggio offerto dall'utilizzo di modelli parametrici, a cui la ricerca ha dato ultimamente particolare attenzione.

In questo lavoro sviluppiamo un modello parametrico e CAD nativo di una chitarra completa, che consenta facilmente il controllo sulle caratteristiche geometriche tipicamente modificate durante un vero processo di costruzione. In particolare, ci concentriamo sulla parametrizzazione della forma e delle barre di rinforzo della tavola armonica. Inoltre, utilizziamo questo nuovo modello parametrico per condurre una serie di simulazioni basate sul Metodo degli Elementi Finiti. In questo modo analizziamo l'effetto di alcune comuni variazioni geometriche, quando queste vengono applicate su un modello di chitarra completo, includendo anche l'effetto dell'aria circostante. L'effetto è valutato sia osservando le variazioni delle frequenze naturali che la risposta in frequenza dello strumento, in forma di ammettenza meccanica del ponte e suono irradiato.

Le nostre conclusioni sono in linea con gli studi precedenti, dimostrando la validità del nostro approccio, ma presentano anche alcuni risultati inediti. In particolare, dimostriamo che le barre trasversali della tavola armonica sottostanti alla tastiera non svolgono alcun ruolo significativo né nel determinare il timbro dello strumento né nel migliorarne l'efficienza di radiazione. Nel fare ciò, mostriamo anche come il nostro modello può essere utilizzato per facilitare future ricerche sulla fisica della chitarra.

Parole chiave: acustica musicale, chitarra, modellazione parametrica, analisi modale, metodo degli elementi finiti, risposta in frequenza

Contents

Introduction

The history of guitar making has predominantly followed traditions and methods that draw from the luthier's intuition and personal skill, rather than adhering to formalized and rigorous rules. Even in today's era of technological and scientific progress, tradition still holds sway in the guitar making process. This is understandable given the intricate nature of the instrument, which involves multiple branches of physics, making its study a formidable challenge even for scientists and engineers alike. Which geometrical or material features determine the quality of an instrument is probably the most debated matter among makers, but also one that is seldom approached with a scientific mindset.

Traditionally, guitar makers have employed the tap-tuning method to get a qualitative estimation of the top plate resonances and thus perform the necessary adjustments to the geometry. Another simple and widely available method to study the modal shapes and frequencies of a guitar plate is the use of Chladni patterns. More recent methods, which fall under the general framework of modal testing, aim at estimating the FRF (Frequency Response Function) of the instrument at various points through the use of sensors, hammers, shakers or less invasive instruments as in the case of holographic interferometry. These experimental methods are still the best option to measure existing instruments, and the results obtained with them can certainly provide some general guidelines in the construction process. However, as they rely on the availability of an actual physical instrument to be measured, they are not particularly useful if we wish to create models that can somehow predict how an instrument will behave from its construction features. With the rise in computational power, numerical simulations have become an increasingly feasible option for studying musical instruments, not only for prototyping individual pieces but also to generate and test multiple models in a relatively short amount of time. The large amount of data gathered in this way can help in fueling a more scientific and mathematical approach to instrument making, by framing it as an optimization problem depending on the desired target qualities.

For these methods to yield reliable results an accurate representation of the instrument is paramount, which can be obtained either through CAD software, 3D scanning of a real object or directly by sampling points from some equation that describes the geometry. In

the latter case the model will be naturally parametric, while different CAD software allow the parameterization of their designs to different degrees. It is clear that the availability of a fully detailed and parametric model can greatly facilitate this type of research.

Starting from a guitar model which was initially developed in Fusion 360® by Lercari to study the use of mechanical metamaterials in guitar top plates ([1, 2]), the goal of this thesis is to parameterize its shape, enabling convenient control over the geometrical features which are considered key in the context of guitar making. Through the use of Fusion 360® and simulation software APIs, it is also possible to create a streamlined and automated process for the generation and simulation of multiple models.

Additionally, we utilize our new parametric model to conduct simulations based on the Finite Element Method (FEM) inside COMSOL Multiphysics®. We initially compute the natural frequencies of the instrument and analyze how these change when modifying various geometrical parameters. Subsequently, we measure the mobility at the bridge and the SPL (Sound Pressure Level) near the instrument when the soundboard is driven at different frequencies. These simulations serve both to showcase the possibilities of our model and to hopefully provide guidance for further studies on the physics of guitars.

1 | State of the Art and Theoretical Background

In this chapter we cover the main concepts and previous studies necessary for understanding our work and placing it in the appropriate context. Section 1.1 gives a quick rundown of the main parts of a classical guitar and their names. Section 1.2 provides an overview of the relevant literature, and how our work relates to it in terms of originality. Section 1.3 introduces the main theoretical concepts that were employed in our studies.

1.1. Components of a Classical Guitar

Probably influenced by other medieval chordophones, such as the oud and the lute, the early history of the guitar is difficult to track. However, its modern and well-known design is commonly attributed to a group of Spanish makers who operated in the 19th century, most notably Antonio de Torres Jurado, who is credited for the introduction of many important features (such as the fan-braced strutting pattern).

A diagram illustrating the design of a typical classical guitar, with its most important components, can be seen in Figure 1.1.

The lower part, encompassing the soundboard, sides (also called *ribs*) and back plate, along with their related structural elements, is also known as the guitar *body*, to distinguish it from the neck and fretboard section.

While the neck and fretboard obviously play a significant role in supporting the strings and allowing the instrument to be played, the body is what serves as the main resonator. As such, its geometrical and material characteristics are fundamental in shaping the overall sound of the instrument.

In particular, great care is devoted to the construction of the soundboard (also known as *top plate*), which is supported by the addition of multiple wooden struts, forming what is known as *guitar bracing*. The design of these bars is crucial as they should increase the

stiffness of the plate, avoiding distortion caused by the strings tension over time, while still allowing it to resonate properly.

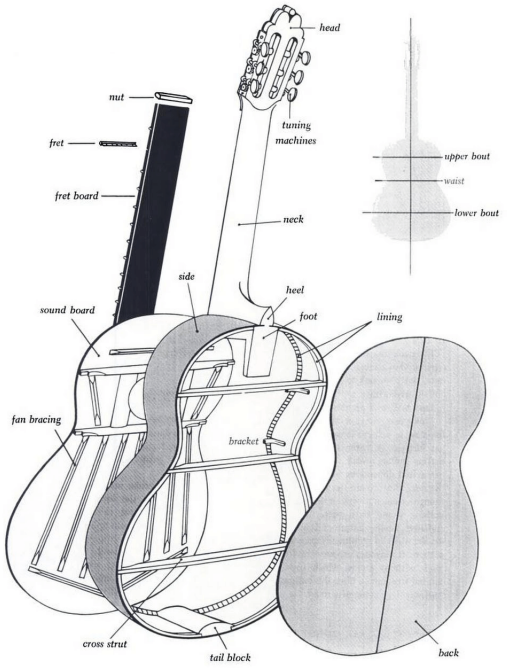

Figure 1.1: Exploded view of a guitar with its main components, from [3].

While some form of fan bracing is present in almost all classical guitars, the design in the upper bout area can vary more significantly. Consequently, some of the bars in this region do not have commonly agreed-upon names. The names used in the following chapters are defined for easier reference throughout the text but may not find correspondence in the existing literature.

1.2. Literature Overview

While the literature on musical acoustics, particularly stringed instruments, has been active for over a century, research specific to the guitar remains relatively scarce, especially when compared to other instruments like the violin. Nevertheless, the existing general literature forms a solid foundation, allowing us to delve deeper into the unique details of this instrument.

When it comes to experimental modal testing, some early studies applying modern techniques like holographic interferometry for the study of guitars can be found in [4] and [5]. The chapter on guitars in Fletcher and Rossing's book also serves as a quite comprehensive summary of the scientific research conducted on the instrument, at least up until the close of the 20th century [6]. Most of the research utilizing FEM for the modal analysis

of guitars is instead quite recent, though there are early studies even dating back to the 1980s [7]. A general review of FEM-based studies of string instruments can be found in [8].

Some recent works have used FEM techniques to delve into the impact of geometric or material variations on the modes of guitar or violin plates [2, 9–12]. In this context, particular effort is now being devoted to the development of parameterized models, allowing to establish a functional relation between the construction features and the vibroacoustic characteristics of the instrument [9, 10, 13].

Compared to previous models like the one employed in [10], an advantage of having a CAD native parametric model like ours is that it can be directly used to drive CNC routers or 3D printers, allowing for easier experimental validation of the numerical results.

It is further worth emphasizing that our analyses are conducted on a complete guitar, including the neck and fretboard, and also account for the influence of surrounding air on the instrument's characteristics. Notably, the body of published studies on this subject considering a similar setup is still quite limited at the current state of the art. Many works only consider a limited set of features, often focusing just on the top plate of the instruments or neglecting the fluid-structure interaction [8]. The coupling of the guitar body with the air enclosed in the soundbox was analyzed (using both Finite Element analysis and experimental methods) in [14, 15], though the effect of the surrounding air was not included. While the top plate effectively plays a dominant role in shaping the instrument sound, and studying it in isolation can offer valuable insights, the effect of air and other structural components have been possibly downplayed in a lot of research to date. The way the top plate couples with the air enclosed in the soundbox and, through it, with the back plate, greatly influences the lower modes [16]. Additionally, a significant amount of sound energy is also radiated by the soundhole and the back plate in the low frequency range [6, 17]. By explicitly modeling the propagation through air, we can also compute the sound intensity at any point inside the domain, or estimate the radiation pattern of the instrument. Finally, when studying the effect of geometrical or material variations, it is easy to overestimate their impact when only the top plate is considered [18].

The simulation setup presented here takes inspiration, in particular, from the work conducted on archtop guitars by Longo et al. [18]. In that case, FEM analysis was run on a guitar model complete of ribs and back plate, and also accounted for the effect of the surrounding air. Furthermore, the boundaries of the air domain were modeled using the spherical wave radiation condition, aligning with the approach adopted in this study.

A very similar setup to our own was also used to study the vibrations and radiation of the kantele, a traditional Finnish string instrument [19].

1.3. Theoretical Background

In this section we provide a brief overview of the main theoretical concepts underpinning our work. We start by introducing modal analysis in the simplest scenario (Single Degree of Freedom discrete systems) and then generalize it until we arrive at how eigenmodes and eigenfrequencies are obtained for continuous solids. Later, we provide the equations that describe wave propagation through air and the interaction of air with vibrating solids. Emphasis is placed on the actual equations that will be solved using FEM, of which a very brief summary is given towards the end.

1.3.1. Modal Analysis

Modal analysis is the study of the dynamical properties of an object in the frequency domain, which is usually described in terms of its eigenfrequencies, damping factors and modal shapes.

Single-Degree-of-Freedom systems

For a system composed of a single mass m, a spring of stiffness k and a damper, characterized by the damping coefficient c, the equation of motion reads

$$m\ddot{u} + c\dot{u} + ku = f(t) \tag{1.1}$$

where $f(t)$ is the applied force and $u(t)$ is the displacement of the mass. This is often referred to as a Single-Degree-of-Freedom (SDOF) system. If we wish to study its behaviour in the frequency domain, we can take the displacement u to be harmonic with frequency ω

$$u = \tilde{u}e^{j\omega t} \tag{1.2}$$

where $\tilde{u}$ is the (generally complex) displacement amplitude.

In the context of modal analysis, the external force term $f(t)$ is often neglected to study the system's own natural oscillations, known as *free vibrations*. In this way we obtain the following equation

$$(-\omega^2 m + j\omega c + k)\tilde{u}e^{j\omega t} = 0 \tag{1.3}$$

where the non-trivial solutions are given by

$$\omega_{1,2} = \omega_0(j\zeta \pm \sqrt{1-\zeta^2}) = j\lambda \pm \omega_d \tag{1.4}$$

where

$$\omega_0 = \sqrt{\frac{k}{m}}, \qquad \zeta = \frac{c}{2\sqrt{km}} \tag{1.5}$$

The real part of the result, $\omega_d = \omega_0\sqrt{1-\zeta^2}$, represents the oscillatory (periodic) component of the displacement, while the imaginary part $\lambda = \omega_0\zeta$ represents the damping part, which describes how fast the motion will decay over time. The quantity ζ is also called the damping ratio and can be rewritten as

$$\zeta = \frac{\lambda}{\omega_0} = \frac{\lambda}{\sqrt{\lambda^2+\omega_d^2}} \tag{1.6}$$

It is clear that when $\zeta > 1$ the oscillatory component becomes imaginary as well and thus no actual oscillation can occur (the system is said to be *overdamped*).

In a SDOF system, the mass can move in only one way and thus there is just one modal shape and corresponding eigenfrequency.

Multi-Degree-of-Freedom systems

When we have more moving masses, a single value is not enough to describe the motion of the overall system. In this case we talk of a Multi-Degree-of-Freedom system (MDOF), whose motion is described in general by

$$\mathbf{M\ddot{u}} + \mathbf{C\dot{u}} + \mathbf{Ku} = \mathbf{f}(t) \tag{1.7}$$

Repeating the same passages done for the SDOF case, we now arrive at the following matrix equation

$$(-\omega^2\mathbf{M} + j\omega\mathbf{C} + \mathbf{K})\tilde{\mathbf{u}}e^{j\omega t} = \mathbf{0} \tag{1.8}$$

which forms an eigenvalue problem, whose solutions can be found by equating

$$\det\left(-\omega^2\mathbf{M} + j\omega\mathbf{C} + \mathbf{K}\right) = 0 \tag{1.9}$$

In general the number of solutions (i.e. of eigenfrequencies ω) will be N for a system with N degrees of freedom. For each eigenfrequency ω_i $(i = 1, .., N)$ we will also have a corresponding eigenmode $\tilde{\mathbf{u}}_\mathbf{i}$, which describes the amplitude of each individual mass

oscillation. The presence of a complex eigenmode indicates that different masses move with different phase offsets.

Continuous systems

For continuous systems the displacement is represented by a displacement field $\mathbf{u(x)}$, where $\mathbf{x}$ is the position in space, and so are the eigenmodes $\mathbf{u_i(x)}$. Since these systems have infinite degrees of freedom, theoretically the number of eigenmodes and eigenfrequencies is infinite as well, though in most cases only the lower ones are of practical interest. Additionally, techniques like the FEM involve a discretization process that converts the continuos system into a discrete MDOF one, so the number of eigenmodes will be in any case bounded by the number of discrete elements.

For continuous systems, the expression of the displacement depends upon the particular material and the model used to describe it. In particular, the theory of linear elasticity is often employed when dealing with small deformations in solids.

1.3.2. Linear Elasticity

Linear elasticity is a model that describes how elastic solid objects deform under the effect of an external load. It lies on the fundamental assumptions that the deformations are infinitesimal and that there is a linear relationship between stress and strain.

Linear elastic materials are governed by the following three equations [20]:

- Constitutive equation

$$\boldsymbol{\sigma} = \mathbf{C} : \boldsymbol{\varepsilon} \tag{1.10}$$

  where $\boldsymbol{\sigma}$ is the Cauchy stress tensor, $\boldsymbol{\varepsilon}$ is the infinitesimal strain tensor, and $\mathbf{C}$ is a fourth-order tensor commonly known as the *stiffness tensor*. The : symbol indicates the double dot tensor product. This can be seen as a generalized version of Hooke's law, applied to continuous media.

- Strain-displacement equation

$$\boldsymbol{\varepsilon} = \frac{1}{2}\left[\boldsymbol{\nabla}\mathbf{u} + (\boldsymbol{\nabla}\mathbf{u})^{\mathrm{T}}\right] \tag{1.11}$$

  where $\mathbf{u}$ is the displacement vector.

- Equation of motion

$$\boldsymbol{\nabla} \cdot \boldsymbol{\sigma} + \mathbf{F} = \rho\ddot{\mathbf{u}} \tag{1.12}$$

which is an application of Newton's second law, where $\mathbf{F}$ is the force per unit volume, and ρ is the density.

Starting from these equations and appropriate boundary conditions, one can determine the displacement $\mathbf{u}$.

The expression and values of the stiffness tensor $\mathbf{C}$ depend on the type of material and its parameters. In practice, due to symmetries of $\boldsymbol{\sigma}$, $\boldsymbol{\varepsilon}$ and $\mathbf{C}$, only 21 components (out of the theoretical $3^4 = 81$) at most are independent in $\mathbf{C}$. This allows us to rewrite $\mathbf{C}$ as a symmetric 6×6 matrix:

$$\mathbf{D} = \begin{bmatrix} D_{11} & D_{12} & D_{13} & D_{14} & D_{15} & D_{16} \\ D_{12} & D_{22} & D_{23} & D_{24} & D_{25} & D_{26} \\ D_{13} & D_{23} & D_{33} & D_{34} & D_{35} & D_{36} \\ D_{14} & D_{24} & D_{34} & D_{44} & D_{45} & D_{46} \\ D_{15} & D_{25} & D_{35} & D_{45} & D_{55} & D_{56} \\ D_{16} & D_{26} & D_{36} & D_{46} & D_{56} & D_{66} \end{bmatrix} = \begin{bmatrix} C_{1111} & C_{1122} & C_{1133} & C_{1112} & C_{1123} & C_{1113} \\ C_{1122} & C_{2222} & C_{2233} & C_{2213} & C_{2223} & C_{2213} \\ C_{1133} & C_{2233} & C_{3333} & C_{3312} & C_{3323} & C_{3313} \\ C_{1112} & C_{2212} & C_{3312} & C_{1212} & C_{1223} & C_{1213} \\ C_{1123} & C_{2223} & C_{3323} & C_{1223} & C_{2323} & C_{2313} \\ C_{1113} & C_{2213} & C_{3313} & C_{1213} & C_{2313} & C_{1313} \end{bmatrix} \tag{1.13}$$

where the subscripts of $\mathbf{C}$ and $\mathbf{D}$ follow the standard material data ordering:

$$\begin{bmatrix} 11 \\ 22 \\ 33 \\ 12, 21 \\ 23, 32 \\ 13, 31 \end{bmatrix} \leftrightarrow \begin{bmatrix} 1 \\ 2 \\ 3 \\ 4 \\ 5 \\ 6 \end{bmatrix} \leftrightarrow \begin{bmatrix} x \\ y \\ z \\ xy \\ yz \\ xz \end{bmatrix} \tag{1.14}$$

Thus we can rewrite the constitutive equation in a simpler matrix form:

$$\begin{bmatrix} \sigma_x \\ \sigma_y \\ \sigma_z \\ \sigma_{xy} \\ \sigma_{yz} \\ \sigma_{xz} \end{bmatrix} = \mathbf{D} \begin{bmatrix} \varepsilon_x \\ \varepsilon_y \\ \varepsilon_z \\ 2\varepsilon_{xy} \\ 2\varepsilon_{yz} \\ 2\varepsilon_{xz} \end{bmatrix} \tag{1.15}$$

Isotropic materials

Isotropic materials are the simplest to study, since their properties do not depend on the direction in which the force is applied. In other words, they have an infinite number of planes of symmetry. In this case the expression of **D** becomes [21]:

$$\mathbf{D} = \frac{E}{(1+v)(1-2v)} \begin{bmatrix} 1-v & v & v & 0 & 0 & 0 \\ v & 1-v & v & 0 & 0 & 0 \\ v & v & 1-v & 0 & 0 & 0 \\ 0 & 0 & 0 & \frac{1-2v}{2} & 0 & 0 \\ 0 & 0 & 0 & 0 & \frac{1-2v}{2} & 0 \\ 0 & 0 & 0 & 0 & 0 & \frac{1-2v}{2} \end{bmatrix} \tag{1.16}$$

In particular this depends only on 2 material parameters:

- The Young's modulus E.
- The Poisson ratio v.

Orthotropic materials

Orthotropic materials are a subset of anisotropic materials whose properties depend on the direction of the applied force. In particular, they have three planes of symmetry. If we assume that their planes of symmetry are aligned with the planes of a cartesian coordinate system, we can write [21]

$$D = \begin{bmatrix} D_{11} & D_{12} & D_{13} & 0 & 0 & 0 \\ D_{12} & D_{22} & D_{23} & 0 & 0 & 0 \\ D_{13} & D_{23} & D_{33} & 0 & 0 & 0 \\ 0 & 0 & 0 & D_{44} & 0 & 0 \\ 0 & 0 & 0 & 0 & D_{55} & 0 \\ 0 & 0 & 0 & 0 & 0 & D_{66} \end{bmatrix} \tag{1.17}$$

where the coefficients are given by:

$$\begin{aligned} D_{11} &= \frac{E_x^2\left(E_z v_{yz}^2 - E_y\right)}{\Delta}, \quad D_{12} = -\frac{E_x E_y\left(E_z v_{yz} v_{xz} + E_y v_{xy}\right)}{\Delta} \\ D_{13} &= -\frac{E_x E_y E_z\left(v_{xy} v_{yz} + v_{xz}\right)}{\Delta}, \quad D_{22} = \frac{E_y^2\left(E_z v_{xz}^2 - E_x\right)}{\Delta} \\ D_{23} &= -\frac{E_y E_z\left(E_y v_{xy} v_{xz} + E_x v_{yz}\right)}{\Delta}, \quad D_{33} = \frac{E_y E_z\left(E_y v_{xy}^2 - E_x\right)}{\Delta} \\ & D_{44} = G_{xy}, \quad D_{55} = G_{yz}, \quad \text{and } D_{66} = G_{xz} \end{aligned} \tag{1.18}$$

where

$$\Delta = E_y E_z v_{xz}^2 - E_x E_y + 2 v_{xy} v_{yz} v_{xz} E_y E_z + E_x E_z v_{yz}^2 + E_y^2 v_{xy}^2 \tag{1.19}$$

In this case we have 9 independent material parameters:

- 3 Young's moduli: E_x, E_y and E_z.
- 3 Poisson ratios: v_{xy}, v_{yz} and v_{xz}.
- 3 shear moduli: G_{xy}, G_{yz} and G_{xz}.

Wood is an example of an orthotropic material, as its mechanical properties are greatly affected by the orientation of the grain lines with respect to the applied load. When building guitars, both the plates and the struts are usually made from *quarter sawn* pieces of wood, which are cut so that the growth rings are approximately perpendicular to the face of the wood. The way this type of cut is obtained, and the corresponding axes of symmetry are shown in Figure 1.2. In this context the three directions are usually called: longitudinal (direction along the grains), radial (direction along the radius of the growth rings) and tangential (direction tangential to the growth rings). Thus the material properties are also specified according to these directions; for example the Young's moduli are given as E_L, E_T and E_R.

The orientation of grain lines in the soundboard significantly influences the structural integrity and vibrational behavior of the instrument. Traditionally, guitar makers have predominantly adhered to a common approach, aligning the grain lines parallel to the direction of the strings. Therefore, it is crucial to accurately model the orthotropic behavior of this component. In contrast, how the ribs and back are carved from the original wood piece is often viewed as a more subjective and aesthetic choice. Makers frequently hold diverse opinions on this matter, generally concurring that its impact on the overall instrument is comparatively minimal. For this reason, these components have been modeled in different ways or simply as isotropic in previous studies.

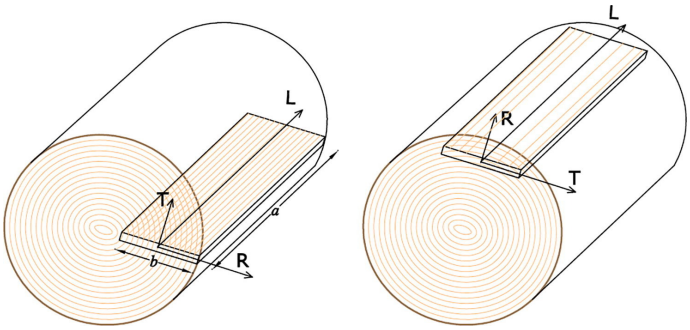

Figure 1.2: Diagram illustrating how a *quarter sawn* (left) and *plain sawn* planks are obtained from a log, annotated with their corresponding axes of symmetry (from [22]).

Frequency domain and eigenfrequency study

If the linear elastic material is studied in the frequency domain, then the displacement and the force will be harmonic with the same angular frequency ω, and Equation 1.12 becomes:

$$\boldsymbol{\nabla} \cdot \boldsymbol{\sigma} + \mathbf{F} = -\rho\omega^2\mathbf{u} \tag{1.20}$$

The resulting modal shapes and frequency pairs ($\mathbf{u}$, ω) depend upon the boundary conditions and the external force $\mathbf{F}$. In our case all structural boundaries were considered free, therefore no condition is applied on $\mathbf{u}$. In the case of an eigenfrequency study, if one considers the free vibrations of the system, the force term $\mathbf{F}$ is usually set to zero. However, in our case $\mathbf{F}$ must be considered in the eigenfrequency study too, since it models the load of the surrounding air, as detailed in the next section.

1.3.3. Acoustic-Structure Interaction

The interaction between the instrument structure and the surrounding air happens at many levels. Firstly, the vibrating structure creates pressure waves in the surrounding air; these small oscillations around the static atmospheric pressure are what we perceive as sound. However, the air also influences the eigenfrequencies of the structure in two important ways:

- It applies a pressure load on the structure, altering its eigenfrequencies (usually lowering them).
- The air enclosed in the soundbox has its own modes and thus forms a coupled system with the structure.

The Partial Differential Equation (PDE) we use to describe the pressure field p is the

usual equation for sound waves in a lossless medium:

$$\nabla^2 p - \frac{1}{c^2}\frac{\partial^2 p}{\partial t^2} = 0 \tag{1.21}$$

where $\nabla^2 p = \nabla \cdot (\nabla p)$ is the Laplace operator applied to the pressure field and c is the speed of sound.

When working in the frequency domain, the pressure is assumed to be harmonic in time:

$$p(\mathbf{x}, t) = p(\mathbf{x})e^{j\omega t} \tag{1.22}$$

In this case Equation 1.21 can be rewritten as

$$\nabla^2 p + k^2 p = 0 \tag{1.23}$$

which is commonly known as the homogeneous Helmholtz equation, where $k = \omega/c$ is the angular wavenumber.

Notice that neither of these equations considers the presence of sources in the domain. Instead, the interaction between the fluid and the structure can be modeled by considering two equations at their boundaries:

- The fluid load experienced by the solid structure (force per unit area)

$$\mathbf{F}_{\mathrm{A}} = p \cdot \hat{\mathbf{n}} \tag{1.24}$$

- The boundary condition for the fluid pressure, affected by the structural acceleration $\ddot{\mathbf{u}}$

$$\hat{\mathbf{n}} \cdot \frac{1}{\rho}\nabla p = -\hat{\mathbf{n}} \cdot \ddot{\mathbf{u}} \tag{1.25}$$

  where $\hat{\mathbf{n}}$ is the surface normal.

1.3.4. Acoustic Boundary Conditions

Since the domain of the surrounding air is finite, we must also properly model its boundaries to avoid reflections of the outgoing pressure waves as much as possible, thus approximating a free-field propagation. The two commonly employed methods to achieve this are perfectly matched layers (PML) or absorbing boundary conditions (ABC), which work by absorbing the incoming wave [23]. In this case we use the latter, which is usually

formulated as

$$\hat{\mathbf{n}} \cdot \left(\frac{1}{\rho} \nabla p(\mathbf{x}, t) \right) = -\frac{1}{\rho c} \frac{\partial p(\mathbf{x}, t)}{\partial t} - \frac{R(r)}{\rho} p(\mathbf{x}, t) \tag{1.26}$$

where r is the distance from the wave origin to the boundary. In the case of spherical waves we have $R(r) = 1/r$, and assuming time-harmonic behaviour the equation can be simplified to

$$\hat{\mathbf{n}} \cdot \nabla p + \left(jk + \frac{1}{r} \right) p = 0 \tag{1.27}$$

This is also sometimes referred to as the spherical wave radiation condition. The above equation is the first-order expansion, but sometimes a second-order expansion is preferred for higher accuracy, which is given by [24, 25]

$$\hat{\mathbf{n}} \cdot \nabla p + \left(jk + \frac{1}{r} \right) p + \frac{r \nabla_{\parallel}^2 p}{2(1 + jkr)} = 0 \tag{1.28}$$

where $\nabla_{\parallel}^2 p$ denotes the Laplace operator in the tangent plane at a particular point.

1.3.5. Finite Element Method

Many physical phenomena are described by partial differential equations (PDE) which, when defined on complex geometries, become impossible to solve with analytical methods. This is the case, for example, of Equation 1.12. The goal of FEM is to reformulate a problem defined by a differential equation as a set of algebraic equations, which can be solved numerically.

Assuming we need to find a function $u : \Omega \to \mathbb{R}$ described by a PDE, the main steps performed by FEM are [26]:

1. Find a *weak formulation* of the problem. This usually involves integrating the equation over its domain and multiplying it by a *test function*. In this way the equation is not required to hold absolutely but only with respect to all test functions in a function space V. In the *Galerkin method* we also assume that the solution belongs to the same function space V.

2. The continuous domain Ω is discretized into a finite number of *nodes*, which correspond to the vertices of the geometric primitives (e.g. tetrahedrons in the case of 3D domain) used to subdivide it; this process is known as *meshing*. A basis function ϕ_i is associated with each node $i = 1, ..., N$.

3. Instead of finding u, we find an approximation u_h which belongs to a finite dimensional subspace $V_h \subset V$, usually the space of piecewise polynomial functions over

the mesh elements. In the case of linear polynomials, the functions of this space can be written as

$$u_h(\mathbf{x}) = \sum_{i=1}^{N} u_i \phi_i(\mathbf{x}) \tag{1.29}$$

4. A system of equations is built where the coefficients u_i form the unknown vector.
5. The boundary conditions are applied.
6. The system is solved numerically.

In this process, a key phase is the meshing (discretization) of the domain, which turns a continuous system into a MDOF system. The choice of the mesh and the basis functions can greatly affect the accuracy of the results.

It is important to emphasize that this method provides approximated solutions, which should be ideally verified with experimental data, obtained for example through modal testing. Though every simulation result should be individually validated, previous studies have shown good agreement between experimental and numerical results in the analysis of guitar plates [9] and other string instruments [27, 28].

1.3.6. Frequency Response and Mobility

The frequency response of a system describes its steady state output in response to a sinusoidal input of varying frequency. In the case of musical instruments, there are many possible ways to define a frequency response, depending on what we consider as input and output. If we only consider its mechanical response, the input usually consists of an applied force $\mathbf{F}$, while the output can be an acceleration, a velocity or a displacement, measured at a specific point. When the frequency response is given as the ratio of velocity to force

$$\mathbf{Y}(\boldsymbol{\omega}) = \frac{\mathbf{v}(\boldsymbol{\omega})}{\mathbf{F}(\boldsymbol{\omega})} \tag{1.30}$$

it is called *mobility*, sometimes also known as *mechanical admittance*. If the velocity is measured at the same point where the force is applied, it is referred to as the *driving-point* mobility. This quantity is particularly important to describe the timbre of stringed instruments, as the sound radiated by a plate-like structure is directly related to its velocity. Since the strings vibrations are transmitted to the soundboard through the bridge, it is customary to measure the mobility there to have an estimate of the entire plate behaviour.

2 | Design of a Parametric Guitar Model

This chapter details how the parametric model was designed and gives a description of the most important implemented parameters. Some of these parameters will be referenced in the next chapters when presenting the simulation results, while others are reported only to describe the model and facilitate its use in future research.

The model presented here was created starting from the one previously developed by Lercari [1], which already includes a guitar body complete of its bracing bars. For this work, we focused on making the geometry of this model parametric. Moreover, we added some details (e.g., tapering and drafting of the braces) and included the guitar neck to obtain a complete model. In the following sections, we only describe the most important features and those that were altered with respect to the original model, while for the other details the reader can refer directly to [1].

The basic design of the model is inspired by one of Antonio de Torres' most popular guitars, according to the specifications described in [29].

2.1. The Soundboard

The soundboard was obtained by first drawing the outline of the plate and then extruding it with a thickness of 2.1 mm. While in real guitars the thickness usually varies throughout the soundboard, here this feature was neglected for simplicity.

2.1.1. Outline

Compared to the original model presented in [1], the outline was redesigned to use a simpler spline curve with fewer control points, which can thus be parameterized and controlled in an intuitive way. In particular, we employed a control point spline with a degree of 5 and 8 control points. The curve was created by visually matching the images of various guitar models that were imported into Fusion 360®.

Although the accuracy of the outlines could have been improved by using more control points, we intentionally used as few as possible to minimize the parameters to control.

Out of the 8 control points, 2 are the endpoints of the spline, leaving 6 individually adjustable points. The positions of the final points change only when altering the total length of the guitar body. Additionally, 3 of these points have fixed heights: one is the waist control point (W), and the other two are the second-to-last points (UB1 and LB2), whose heights are set equal to the endpoints. This ensures smooth continuity at the joint between the two symmetric sides of the outline, guaranteeing at least $C2$ continuity. Figure 2.1 shows the control points, the relative control polygon and the resulting outline curve.

With this model, we focused on reproducing the outlines of three different types of guitars: a traditional classical guitar (our reference Torres model), a jumbo model, and a dreadnought model. The reproduced outlines, shown in Figure 2.2, still deviate from the reference ones by no more than 3 mm. In Figure 2.3 we can see the corresponding 3D guitar models (notice that only the outline shape is recreated, while the bracing system is the same as the base model). The coordinates of the control points used to fit the three guitar models are presented in Table 2.1.

Although the considered models had different body lengths, they were all normalized to a length of 483 mm (the length of the reference Torres model) for simplicity. This normalization does not affect the relative positions of the control points since any outline can be scaled uniformly, preserving its shape, by equally scaling all the positions of the control points.

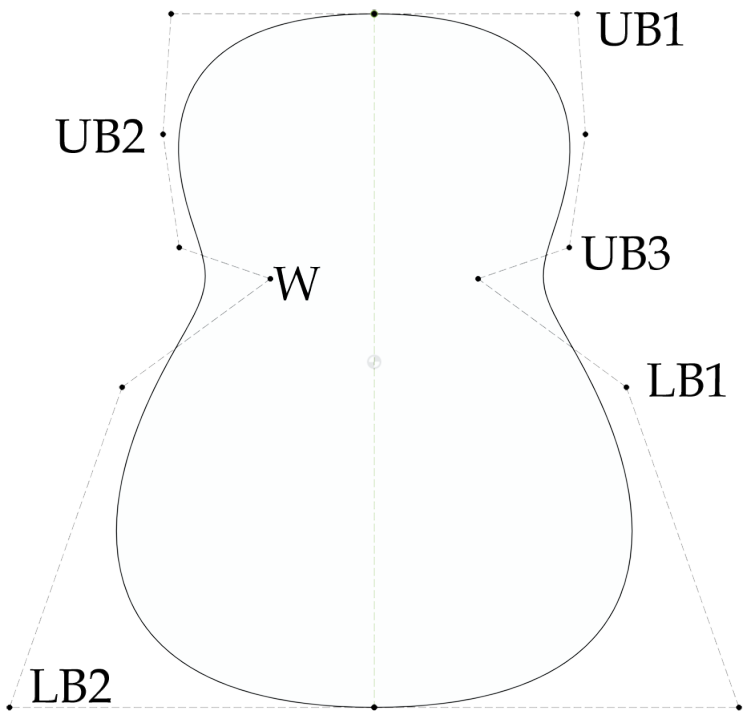

Figure 2.1: Diagram of the simplified spline curve used to fit the guitar outlines, annotated with the parameterized control point names.

Name	**Values (mm)**		
	Torres 1	Jumbo	Dreadnought
x_{UB1}	141.5	197.6	195.2
x_{UB2}	147.1	105.6	95.7
y_{UB2}	83.9	100.3	97
x_{UB3}	135.8	241.4	211
y_{UB3}	162.7	99.6	88.7
x_{W}	72.3	-21.9	1.3
y_{W}	184.5	184.5	184.5
x_{LB1}	175.6	260.1	205.7
y_{LB1}	260	236.6	233
x_{LB2}	254	246.7	246

Table 2.1: Outline parameters for the three considered models. The origin of the coordinate system is located at the topmost endpoint of the spline, and the y-axis runs parallel to the axis of symmetry of the guitar. Therefore, the x-coordinate represents the signed distance from the axis of symmetry in the x-direction, while the y-coordinate represents the distance from the top of the body in the y-direction. The value of y_{W} is reported for completeness although it is not a controllable parameter and its value is fixed for all models.

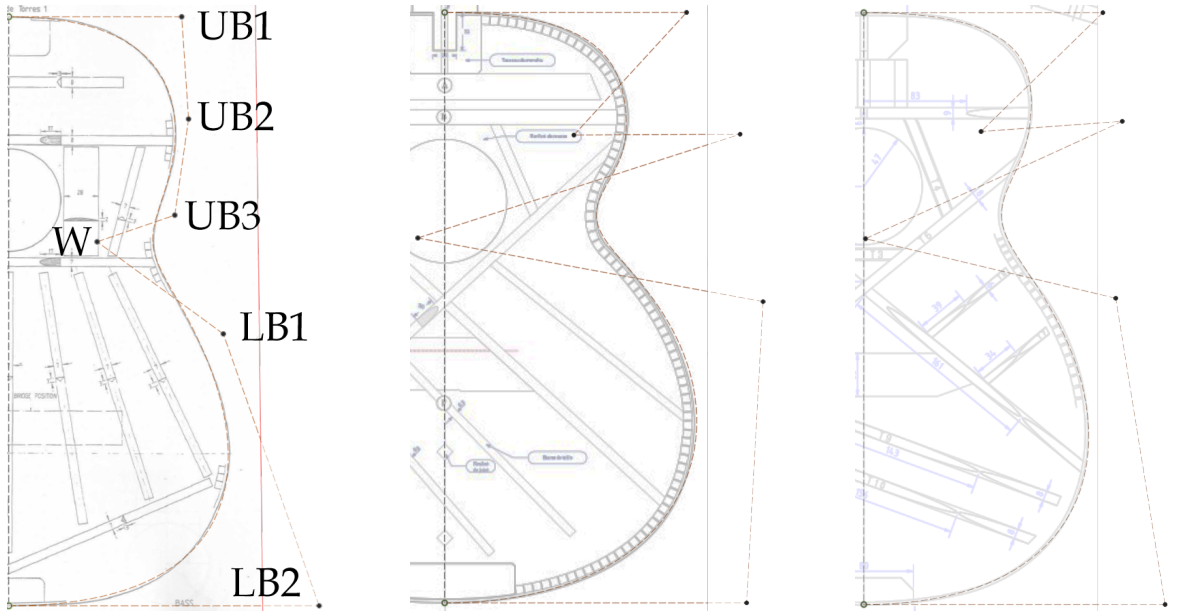

(a) Antonio de Torres classical guitar model 1 (reference model)

(b) Jumbo acoustic guitar model (design by Yves Fesselier)

(c) Dreadnought acoustic guitar model (design by Christophe Grellier)

Figure 2.2: Outlines modeled after three different types of guitar shapes: a traditional classical guitar, a jumbo acoustic guitar and dreadnought acoustic guitar. The approximated outline is represented by the dashed orange curve.

2.1.2. Doming

In many classical guitars the soundboard is not built completely flat, but it is instead designed with a slight doming which usually makes the bridge the most prominent part. The way this is often implemented by the luthier is by gluing the bracing bars while the top is placed on a domed work-board (also known as the *solera*). Often times this doming is described by the contour of a sphere with a given radius.

During the design phase, we carried out some preliminary simulations to determine whether this design feature should be accounted for in our model, or if its effect could be safely neglected. In our model, the doming was obtained by extruding the surface of a sphere with a radius of 9 m, and then intersecting it with the projection of the soundboard outline. For the purpose of this comparison, we only considered a simplified model of the body, devoid of all the bracing bars and fretboard.

The results, presented in Section 3.2, show that this feature has a negligible impact on the eigenfrequencies of the guitar. Therefore, the decision was made to keep the soundboard flat for the sake of design simplicity.

(a) Torres outline model

(b) Jumbo outline model

(c) Dreadnought outline model

Figure 2.3: Complete 3D guitar models for the three different outline shapes seen in Figure 2.2. The soundboard is transparent to show the bracing bars inside.

2.1.3. Bracing

The bracing bars design is the same as described in [1], which follows closely the Torres model. However, the fan bars were slightly moved so that their positions are distributed along a circular pattern with uniform angular spacing. This provides an easy way to control the spread of these bars with a single parameter, which is a feature that often varies between different designs.

Additionally, the original 3D model only included the scalloping of the harmonic bars, while the other struts were modeled with a simple flat top. We improved the model by adding drafting and tapering on all the remaining bars, in order to make their mass and stiffness as accurate as possible. Drafting was performed to give the bars a triangular cross-section, which is a commonly employed profile and is the one found in our reference guitar. The only exceptions are the reinforcing bars next to the soundhole (hereby named *side bars*), which have instead a curved profile that was modeled with a circular arc.

The tapering is usually only found on the fan struts, though the details of this aspect were not specified in the design reference. We implemented this simply by cutting away a right triangular prism at both ends of the fan bars. By default we make the tapering start at 30% of the total bar length, but this has also been added as a customizable parameter.

2.1.4. Parameters

The parameters related to the soundboard internal features are described in Table 2.2 and Figure 2.4. For each parameter we specify:

- A symbolic name (for easier reference throughout the text).
- The name of the parameter inside the Fusion 360® model.
- The default value.
- A general description.

The name letter indicates which type of feature is controlled (e.g. h stands for "height"), while the subscript refers to the particular guitar component (e.g. t refers to the top bar). Notice that the fan bars are indexed starting from the central one and increasing along the circular pattern; symmetrical fan bars share the same index.

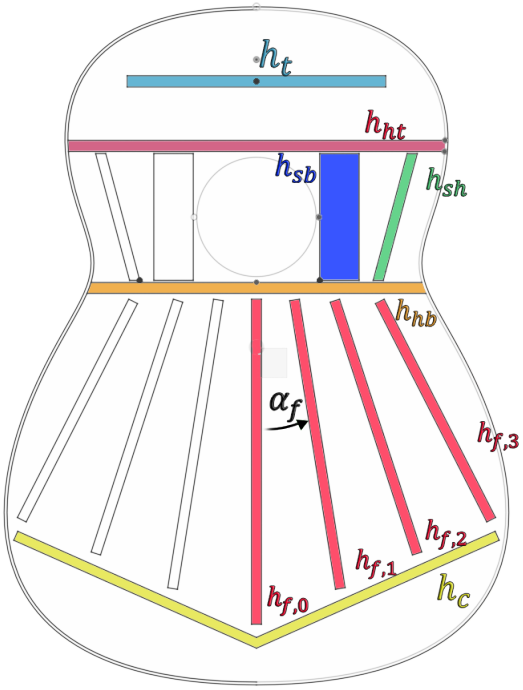

Figure 2.4: Diagram illustrating the geometrical features associated with some of the most relevant soundboard parameters.

Name	Reference value	Fusion 360® name	Description
Soundboard shape			
d_s	85 mm	`soundhole_diameter`	Diameter of the soundhole
t_p	2.1 mm	`top_plate_thickness`	Thickness of the top plate
Braces shape			
$h_{f,i}$	3 mm	`fan_bar_height_i`	Peak height of the fan bars of index i, where $i = 0, ..., 3$
h_t	3 mm	`top_bar_height`	Peak height of the top bar
h_{sh}	3 mm	`soundhole_bars_height`	Peak height of the thin slanted bars in the soundhole section
h_{sb}	2 mm	`side_bars_height`	Peak height of the wider vertical bars around the soundhole
h_c	3 mm	`closing_bars_height`	Peak height of the closing bars
h_{ht}	17 mm	`harmonic_bar_height_top`	Peak height of the top harmonic bar
h_{hb}	17 mm	`harmonic_bar_height_bottom`	Peak height of the bottom harmonic bar
w_f	7 mm	`fan_bars_width`	Width of fan and closing bars
w_t	7 mm	`top_bar_width`	Width of the top bar
t_f	30%	`tapering_amount`	Tapering length of the fan braces (percentage of total bar length)
Bracing layout			
α_f	9°	`fan_angle_spacing`	Uniform angular spacing of the fan braces
α_c	24°	`closing_bars_angle`	Angle of the closing bars

Table 2.2: Table describing the soundboard parameters. We allow for individual control of the most relevant geometrical features but only in a symmetrical fashion.

2.2. Complete Model

2.2.1. The Fretboard

The fretboard model, independently developed by Superbo for another study investigating the effects of scale length and string pre-stress on guitar vibrations [30], was imported into our project and joined with the guitar body. This model also enables parametric control of the scale length; however, throughout our studies we maintained a fixed scale length of 650 mm.

2.2.2. Other Components

The rest of the guitar body (namely the ribs, the back plate along with its bracing, the tailblock and the foot) was adapted directly from [1]. The geometry is thus the same, and the model was for the most part only updated to adjust automatically to the parametric changes in the top plate.

In Table 2.3 we list the parameters which are related to the overall body of the guitar or to components other than the soundboard.

Name	Reference value	Fusion 360® name	Description
t_r	2.1 mm	`ribs_thickness`	Thickness of the ribs
l	483 mm	`total_length`	Total length of the guitar body

Table 2.3: Table describing the geometrical parameters related to the overall guitar shape or components other than the soundboard.

2.3. Material Parameters

This section describes the default material parameters that were used to model the complete guitar body, based on actual materials that are commonly employed by guitar makers. Unless stated otherwise, these are the reference materials used to carry out the Finite Element simulations in COMSOL.

The material associated with each guitar part is displayed in Figure 2.5 and described in Table 2.4, while Table 2.5 contains the values of all the material properties.

For the modeling of bridge and fretboard, slightly unorthodox materials were chosen for practical reasons. Typically these two components are crafted from exotic woods like ebony and rosewood whose material properties are difficult to find, likely due to their scarcity. Walnut fretboards are notably lighter than ebony ones but they can still be found in many classical guitars, especially newer ones, as more environmentally conscious alternatives to exotic woods are being employed. Moreover, the use of walnut in fingerboards is not entirely unprecedented in traditional guitar making, as we can find proof of at least one Torres model that incorporates it [31].

For the parts modeled as isotropic, only the values of the longitudinal Young Modulus E_L and the longitudinal-tangential Poisson's Ratio v_{LT} are to be considered.

Guitar part	Material
Top plate, braces	Engelmann Spruce (orthotropic)
Ribs, back plate, foot, tailblock	Maple (isotropic)
Bridge	Maple (orthotropic)
Neck, head	Mahogany (orthotropic)
Fretboard	Walnut (orthotropic)

Table 2.4: Materials used to model the different guitar parts.

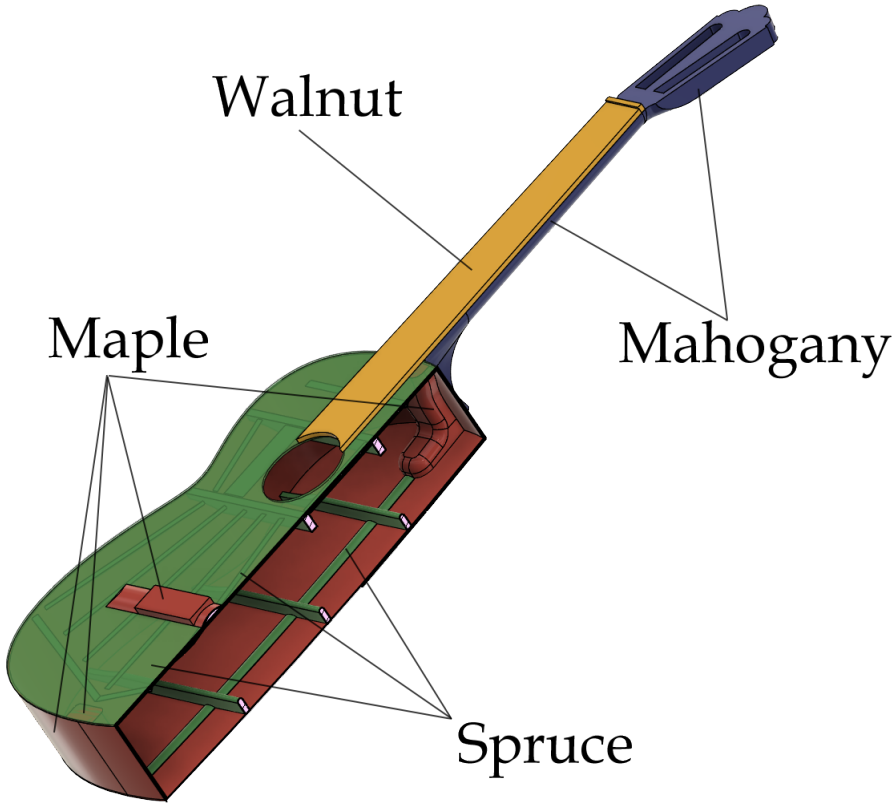

Figure 2.5: Sectional view of the complete guitar model, where the various components have been color-coded depending on the wooden material used to model them.

Density [kg m^3]			
Engelmann Spruce	350		
Red Maple	540		
Mahogany	833		
Walnut	660		
Young's Moduli [GPa]			
	E_L	E_R	E_T
Engelmann Spruce	9.79	1.25	0.58
Red Maple	12.43	1.74	0.83
Mahogany (african)	8.69	0.966	0.434
Walnut	10.78	1.132	0.596
Shear Moduli [GPa]			
	G_{LR}	G_{RT}	G_{LT}
Engelmann Spruce	1.21	0.10	1.17
Red Maple	1.65	0.30	0.92
Mahogany (african)	0.765	0.182	0.513
Walnut	0.916	0.226	0.668
Poisson's Ratios			
	v_{LR}	v_{RT}	v_{LT}
Engelmann Spruce	0.422	0.53	0.462
Red Maple	0.434	0.762	0.509
Mahogany (african)	0.297	0.604	0.641
Walnut	0.495	0.718	0.632

Table 2.5: Values of the material properties used to simulate the complete guitar body, sourced from [32].

3 | Finite Element Analysis

In this chapter we describe the method and the results obtained from the Finite Element Analysis performed on the complete guitar body. Section 3.1 describes the COMSOL simulation setup, Section 3.3 focuses on the modal analysis of the instrument and Section 3.4 on the frequency response (in the form of bridge mobility and SPL).

3.1. COMSOL Simulation Setup

3.1.1. Geometry, Physics and Meshing

The 3D model of the guitar was imported from a STEP file created in Fusion 360®. We employed the *Ignore Edges* function to remove some small edges which can greatly affect the meshing quality, especially in the parts with a more complex geometry (e.g. the neck-soundboard joint and the tailblock). The structural components were modeled using the *Linear Elastic Material* nodes of the *Solid Mechanics* physics interface, which implement the three governing equations of linear elasticity described in Section 1.3.2. The air domain is modeled using the *Pressure Acoustics, Frequency Domain* interface, which solves Equation 1.23. The coupling between the two domains is handled by the multiphysics *Acoustic-Structure Boundary* node, which implements the two equations seen in Section 1.3.3. The air was modeled as a sphere with a radius of 70 cm surrounding the whole guitar, and the domain was partitioned into two: one for the air inside the body and one for the air outside, allowing us to use different mesh sizes for the two domains.

The mesh was obtained using a combination of free tetrahedral elements and swept triangular meshes for the simpler elements with constant cross-section. Due to the large dimensions of the outside air sphere, we use a coarse mesh with a maximum element size of 266 mm. Considering our analyses don't go above 500 Hz, this corresponds to a minimum of approximately 2.5 mesh elements per wavelength. While for most application a minimum of 8 elements is recommended, in this instance we can utilize a lower number since we are not concerned with the modes of this domain. In a preliminary study, we compared the results with those obtained using a finer mesh, featuring 8 elements per

wavelength. This comparison revealed no significant changes in the eigenfrequencies.

3.1.2. Boundary Conditions

For the structural components, all boundaries were considered to be free to move. For the air we employed the *Spherical Wave Radiation* boundary condition, which allows to model a source of spherical waves without having reflections at the boundaries. From a mathematical standpoint, this implements the absorbing boundary condition equations, to the first-order (Equation 1.26) in the case of eigenfrequency studies, and to the second-order (Equation 1.28) for frequency domain studies. The full equation implemented in COMSOL includes an additional optional term that describes an incident pressure field, but this is not used in our scenario.

We positioned the radiation source approximately at the center of the guitar body. While the assumption of modeling the guitar as a source of spherical waves may appear simplistic, a preliminary study demonstrated that using this boundary condition resulted in fewer reflection artifacts compared to using a perfectly matched layer.

3.2. Preliminary Study on Doming

In this section we present the results of the preliminary study that was run to estimate the effect of soundboard doming on the eigenfrequencies.

The results of the eigenfrequency studies are shown in Figure 3.1 and 3.2, where we compare the mode shapes and eigenfrequencies obtained for four different models:

- The reference flat top model.
- The domed top model.
- A flat top model (*model 1*) where the stiffness of the soundboard was increased by 20% in all directions (i.e. all Young and shear moduli were scaled by a 1.2 factor).
- A flat top model (*model 2*) where the stiffness of the soundboard was increased by 15% in the longitudinal and tangential direction and by 7.5% in the radial direction (E_L, E_T and G_{LT} are scaled by 1.15, while E_R, G_{LR} and G_{RT} are scaled by 1.075).

The reason for these two models is that we expect the arching to stiffen the plate more in the longitudinal and tangential direction, since the curvature appears more pronounced along the longitudinal direction. However, the actual radius of curvature is the same in both radial and longitudinal directions, since the doming is obtained through a sphere; it

only appears more pronounced in one direction because of its shorter length.

As we can observe, the effect obtained by doming the top plate is qualitatively similar to the one we get by increasing its stiffness. In particular, the second stiffer model matches the domed one much more closely except for the first two modes, where the first one is more accurate. The first two modes are also the only one where the doming raises the eigenfrequencies more than the stiffening of the plate. Moreover, it is worth noticing how in both cases the mode shapes which involve little motion of the top plate experience a very small change in their corresponding eigenfrequencies. This suggests that the doming of the soundboard could be modeled simply by increasing its stiffness, which is easier to implement when running numerical simulations. Nevertheless, the relative variation in eigenfrequencies produced by the doming is at most around 6%, so the effect of this feature can be neglected for the sake of design simplicity.

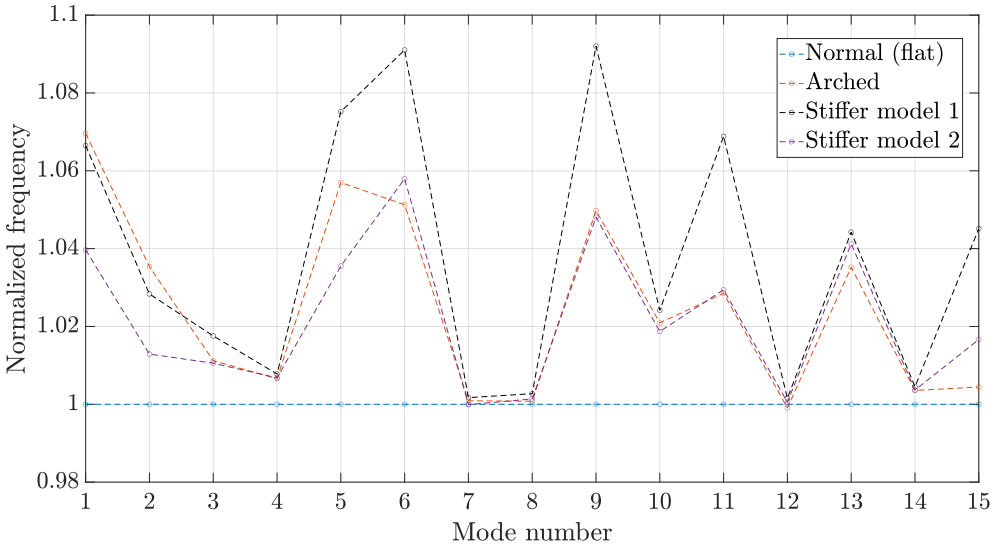

Figure 3.1: Relative eigenfrequencies variation for the first 15 modes obtained when doming or stiffening the top plate.

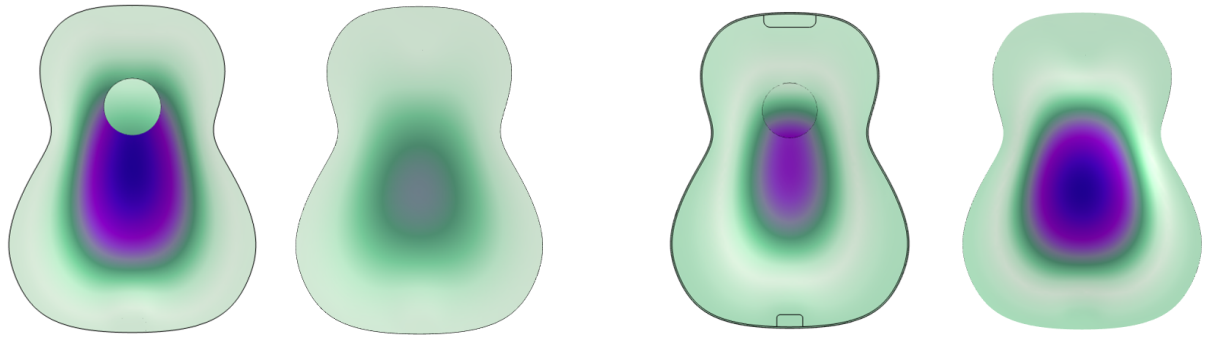

(a) Mode 1

(b) Mode 2

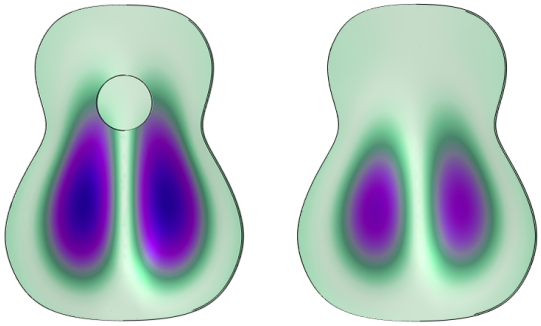

(c) Mode 5

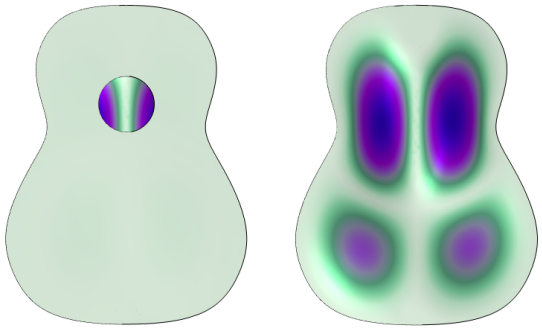

(d) Mode 7

Figure 3.2: Some of the mode shapes corresponding to the eigenfrequencies shown in Figure 3.1. The results shown here refer to the model with the flat soundboard, but the same mode shapes are obtained for the other stiffer or domed models. Notice how mode 7 shows very little motion of the top plate.

3.3. Eigenfrequency Study

(a) Mode 1 (90.371 Hz) (b) Mode 2 (104.38 Hz) (c) Mode 3 (167.54 Hz)

(d) Mode 4 (204.07 Hz) (e) Mode 5 (228.46 Hz) (f) Mode 6 (268.79 Hz)

(g) Mode 7 (300.34 Hz) (h) Mode 8 (312.22 Hz) (i) Mode 9 (317.92 Hz)

Figure 3.3: First 9 modal shapes and eigenfrequencies obtained by simulating the base guitar model (top and back view).

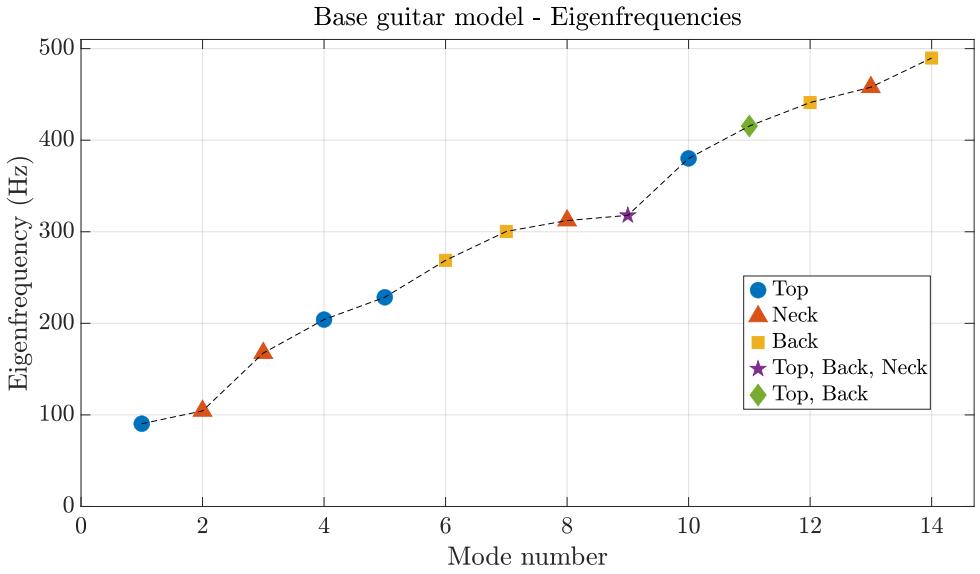

Figure 3.4: The points are colored and shaped differently depending on which parts of the guitar are significantly deformed in that particular mode.

Here we present the results obtained by simulating the eigenfrequencies of the complete guitar body. These results are obtained from the base model, detailed in Chapter 2, and serve as a reference to evaluate the effects of geometrical variations.

The simulation was run for the first 20 eigenfrequencies, but only 14 of them were retained. The 6 discarded modes, in fact, did not represent vibrational modes of the guitar but rather of the air sphere surrounding it, and thus can be considered as artifacts of no interest. Since we expect the real structural modes to have little to no damping, we classified as artifacts all the modes for which the damping ratio satisfied $\zeta > 0.05$.

The remaining first 14 eigenfrequencies are plotted in Figure 3.4, while the modal shapes corresponding to the first 9 are shown in Figure 3.3. The sides of the guitar, while not visible in the figures, exhibited negligible displacement across all obtained modal shapes. The modal frequencies have been classified depending on which parts of the guitar experience a significant deformation. For this classification, we considered three main parts of the guitar: top plate, back plate and neck (including both the fretboard and the head). In practice, for each mode we compute the maximum displacement for each of the three parts, then we check if the values are above or below 50% of the highest one between the three.

In the following sections we will only focus on the first 9 eigenfrequencies, since higher modes have a lesser impact on the sound radiated by the instruments, and the results obtained through the simulation are also less accurate.

Among these, modes 2, 3 and 8 primarily involve deformation of the guitar head and neck. These modes will thus generally have a negligible contribution to sound radiation. Additionally, we expect that their eigenfrequencies will undergo minimal change when variations are applied to the geometry and bracing of the top plate. The same can be expected for modes 6 and 7, where most of the deformation is happening in the back. The first mode is commonly known as the *breathing mode*, since the top and back plate move with opposite phase, forcing air in and out of the soundhole. This causes a large volume change of the enclosed air, which is commonly associated with efficient sound radiation [16, 33]. Something similar happens for mode 4, though in this case the two plates are moving in phase and thus the volume change is smaller. In both cases, anyway, the top and back plate act like monopolar sources, so we expect them to contribute greatly to the sound radiation.

Another interesting thing to notice is that, despite a much larger displacement in the soundboard, there is still a significant and matching motion of the back in these two modes. In other cases, such as for mode 5, the top and the back plate seem to move independently. This is consistent with what was found in prior studies, that showed how the soundboard and the back couples efficiently through the air in the case of mode 1 and 4, while this coupling is not seen for transversal flexural modes like mode 5 [15, 16]. Including the effect of air in the model is particularly important for correctly estimating the frequencies of the modes where this coupling plays a major role. It is worth noting that the studies cited, as well as much of the existing literature, typically treated the ribs as fixed. In our case, however, they are allowed to move freely, and thus the energy transfer from the top to the back plate can happen through this structural element too, especially at low frequencies [6].

3.3.1. Sensitivity Analysis

A sensitivity analysis was performed to understand which geometrical features have the greatest impact on the eigenfrequencies of the whole body. To achieve this, different models were obtained by increasing individual parameters by small amounts, described in Table 3.1. Notice that different parameters were altered by different amounts to consider changes that could be feasibly applied by guitar makers during the construction process. Two additional models were created by varying multiple parameters at the same time: one by increasing all the fan bars height and the other by enlarging the outline. The latter was obtained by increasing all the control points width by 10%, giving the red outline represented in Figure 3.6. Before comparing the eigenfrequencies, we computed the Modal Assurance Criterion (MAC) to check for the presence of mode swapping [34].

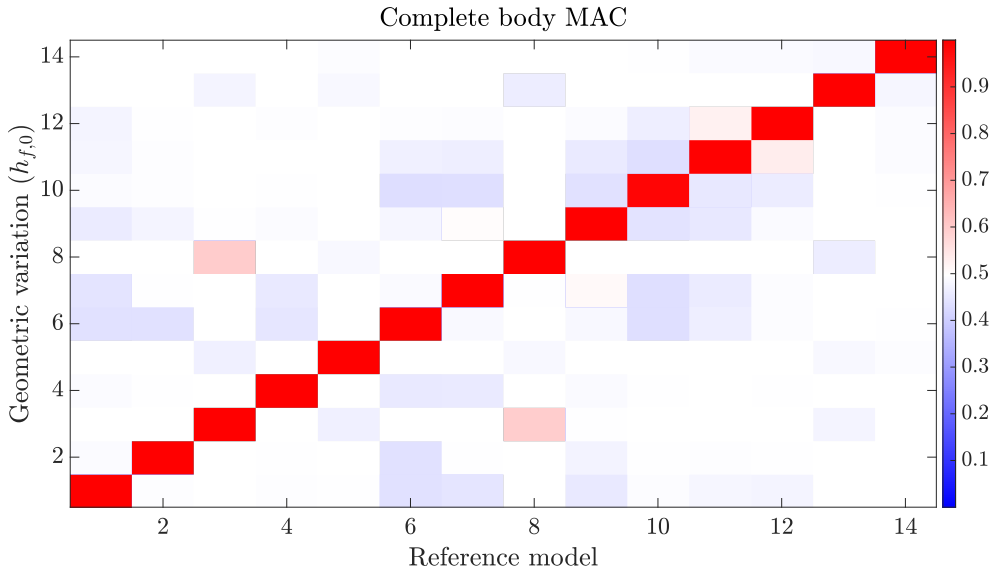

(a) Variation of $h_{f,0}$

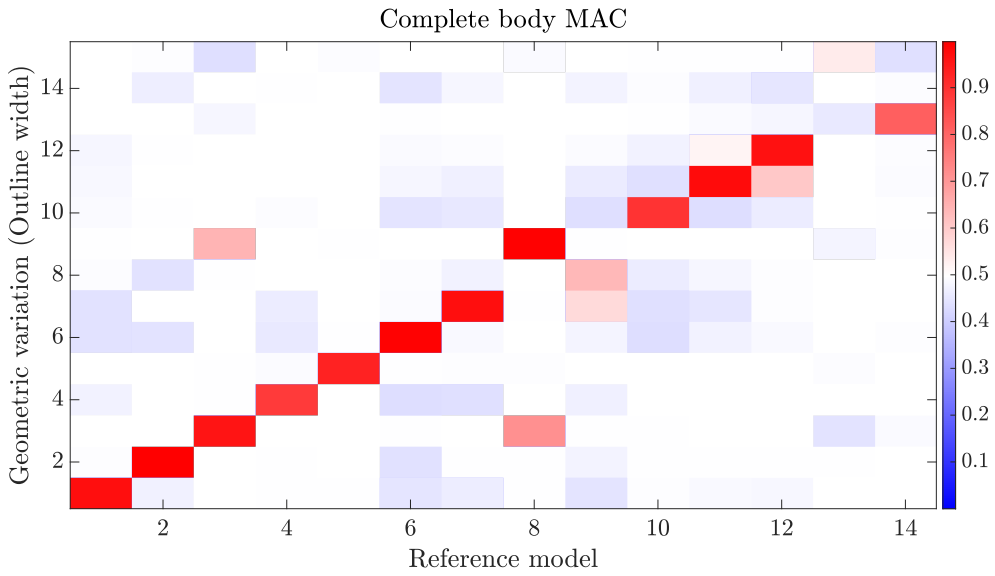

(b) Variation of the body outline width

Figure 3.5: MAC matrix comparing the modal shapes of the reference model and of two selected geometrical variations. Notice that in the case of the outline change the MAC matrix is not square, because a different number of artifact modes were found in the modified model.

Geometrical parameter	Relative variation
$h_{f,i}, h_t, h_{sh}, h_c, h_{ht}, h_{hb}, h_{sb}$	60%
$x_{\mathrm{UB1}}, x_{\mathrm{W}}, t_r$	10%
x_{LB2}	5%

Table 3.1: Relative variations of the geometrical parameters used to perform the sensitivity analysis.

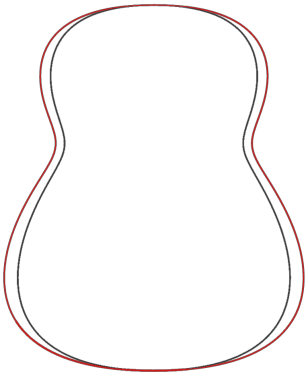

Figure 3.6: Original outline (in black) and wider one (in red) obtained by increasing all the control points width by 10%.

The results are shown in Figure 3.5a and 3.5b for two particular geometrical variations. When applying individual small variations, as in 3.5a, no modal swap was ever observed. The situation becomes more complex if multiple large changes are applied, as is the case for widening the outline seen in Figure 3.5b. The first modal swap occurs due to the significant decrease in the eigenfrequency of mode 9, while the frequency of mode 8, which primarily amounts to neck twisting, remains mostly unchanged.

The result of the sensitivity study is shown in Figure 3.7 in matrix form. The matrix was obtained by varying a set of parameters, simulating the complete body and comparing the resulting eigenfrequencies against those of the reference base model. Except for the last two rows, which consider models with multiple parameter changes, all the others are obtained from models where a single parameter was modified.

Figure 3.8 shows the overall influence I of each geometrical parameter, obtained by summing together the magnitude of the relative variations over the first 9 eigenfrequencies.

As evident upon inspection, modes 1, 4, and 5 exhibit the highest variation. Modes 2, 3, and 8 primarily involve neck bending and twisting, thus remaining largely unaffected by alterations to both the bracing bars and the outline. As expected, modes 6 and 7, which are back-dominated, show minimal sensitivity to changes in soundboard bracing but are influenced by variations in the outline shape. Besides the obvious decrease in

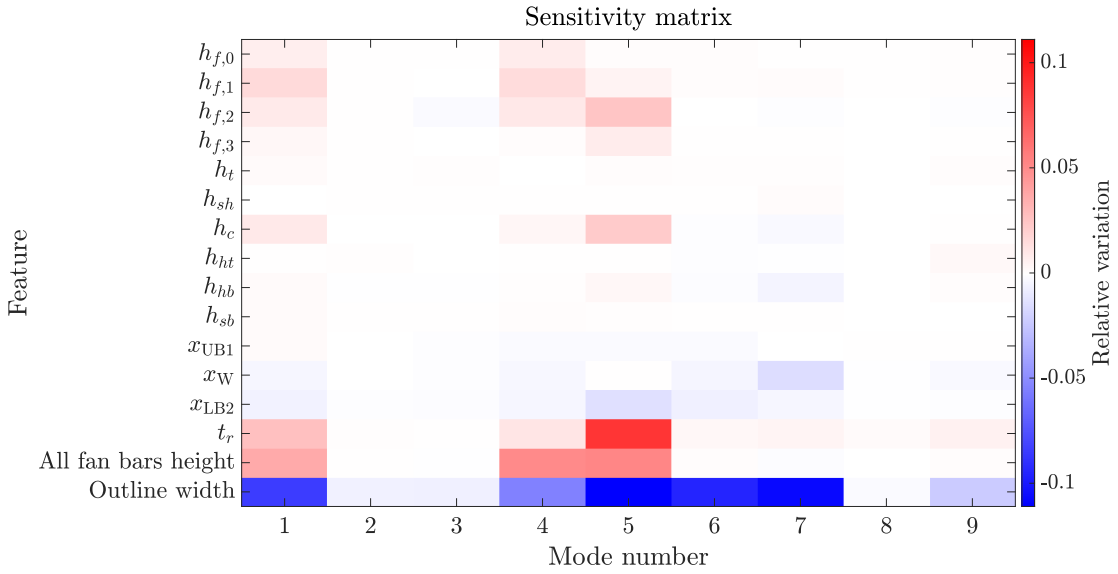

Figure 3.7: Sensitivity matrix representing the relative variations of the first 9 modal frequencies when altering different geometrical features of the guitar body. Each feature is identified by its corresponding parameter variable name, as described in Table 2.1.

frequency due to the enlargement of the vibrating surfaces, increasing the outline also lowers the eigenfrequencies of the air volume enclosed in the soundbox. Thus it will have an additional effect on the structural modes that couple well with the air box modes.

It is noteworthy that the most significantly affected modes are also the most efficient at radiating sound into the surrounding air. This observation underscores the historical significance attributed to some of the analyzed geometric features in shaping the instrument sound.

Simultaneously, it becomes apparent that alterations to the bracing bars in the upper bout have minimal influence on the lower eigenfrequencies. While some of these bars still play a significant role in stiffening the plate, it is possible that some of them may have persisted in guitar design primarily due to longstanding traditions.

Focusing on the fan brace heights, we can observe that the outermost pair of braces ($h_{f,3}$) has the lowest impact on the eigenfrequencies. This is probably because, for the observed modes, most of the deformation happens far from these bars, hence mode 1 and 4 experience little to no change. The other fan bars have comparable effects on these two modes and the greatest difference is found instead for mode 5: here the fan bars closer to the center of the guitar lie near the nodal line of mode 5 and therefore their impact is minimal.

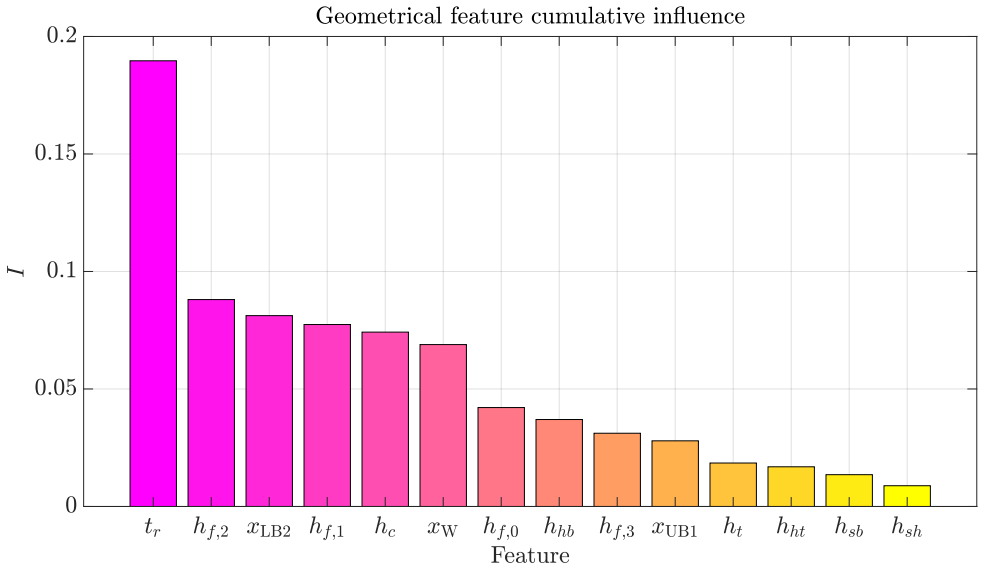

Figure 3.8: Overall influence of each geometrical feature, computed as the sum of the absolute values of the first 9 eigenfrequencies relative variations.

Finally, it appears that increasing the thickness of the ribs exerts the greatest influence on the eigenfrequencies. This effect may be attributed to an increase in the effective stiffness of the ribs, which consequently limits the movement of the top plate along its edges, resulting in higher frequencies. Moreover, stiffer ribs probably reduce the ability of the top and back plate to couple through this component. However, further research should be done to investigate this phenomenon.

3.3.2. Removing the Upper Braces

As we've already mentioned, alterations to bars in the upper bout of the soundboard seem to have little impact on the modal frequencies. The presence of bars located closer to the fretboard also appears hardly justified by their contribution to stiffness, considering the one provided by the fingerboard should be enough to support the top plate in this area. In [30] this claim was already substantiated by showing that removing the upper bars has no significant effect on the stress distribution or the displacement of the soundboard. This phenomenon might have been overlooked in prior, less recent studies employing numerical simulations, due to the fact that the fretboard is often omitted from the models. To analyze if the presence of these bars contributes at least to the dynamic behaviour of the instrument, we tried removing them one at a time and recomputing the eigenfrequencies. Notice that symmetric bars were always removed in pair to maintain the symmetric structure of the instrument. The result is shown in Figure 3.9 for the first

9 modes, while in Figure 3.10 we show the first modal shape for each variation. As we can observe, removing the two bars closest to the fingerboard has very little impact on the first 9 eigenfrequencies (always below a ±2% variation). This is not the case for the other bars closer to the waist line, whose contribution to the plate stiffness is quite significant. Removing these bars seems to make the soundboard a lot more flexible around the soundhole area, shifting the maximum displacement of the modal shape towards this region. In particular, the importance of the lower transversal bar (*hb*) has already been highlighted in previous studies, such as [33].

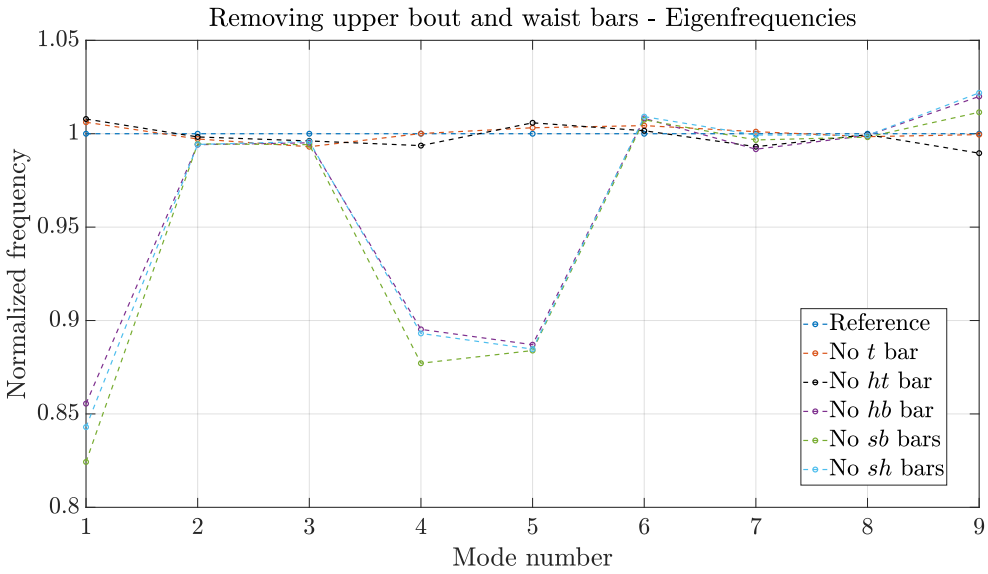

Figure 3.9: Relative eigenfrequency variation for the first 9 modes obtained by removing bars from the upper bout and waist area.

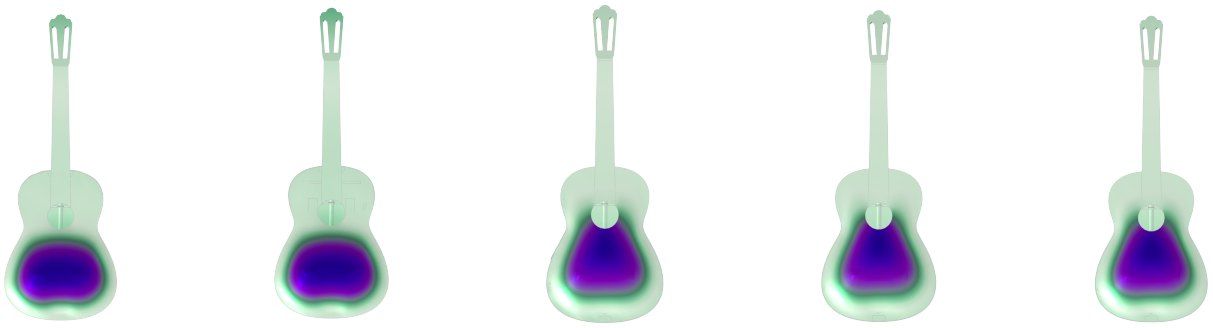

(a) No *t* bar (b) No *ht* bar (c) No *hb* bar (d) No *sb* bars (e) No *sh* bars

Figure 3.10: First modal shape when removing different bars from the upper bout and waist area.

3.3.3. Linearity Study

After measuring the variations due to individual changes in the geometry, we simulated the effects of varying multiple parameters at once. We then compared the result to the one predicted by superimposing the individual changes, to estimate if and which parameters interact in a linear fashion.

Firstly, we evaluated the interaction of changes in the fan brace heights. The results can be seen in Figure 3.11, which shows an almost linear behaviour, though the predicted result tends to slightly overestimate the change in eigenfrequencies. Nevertheless, the two results differ at most by around 2% of the original eigenfrequencies.

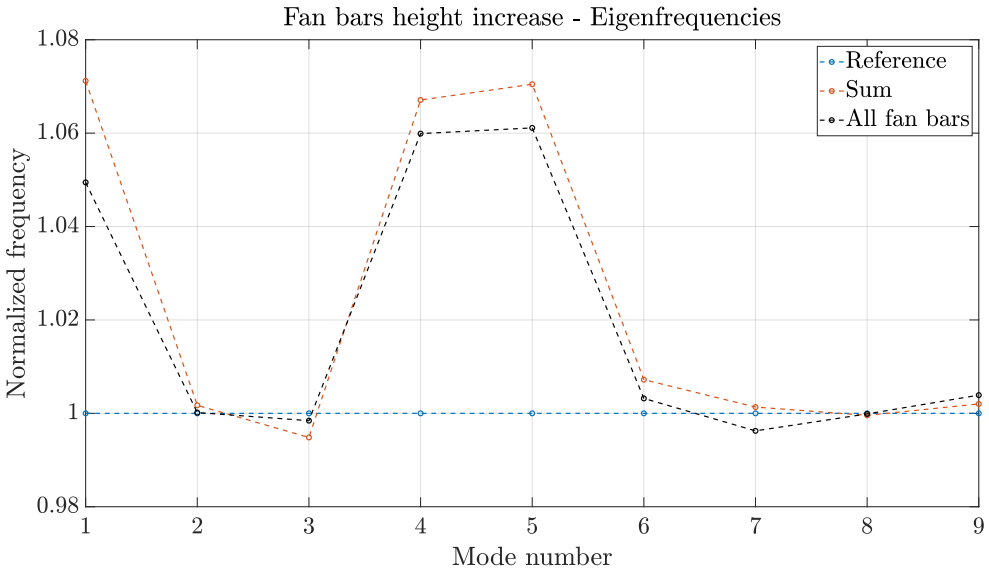

Figure 3.11: Comparison between the relative eigenfrequency variations obtained by increasing all the fan bars by 60% and the result predicted by summing the variations resulting from changing individual bars.

A similar experiment was then run considering the combined effect of the most influential parameters, i.e. those with an overall influence above 5% in Figure 3.8. We added one parameter change at a time (in decreasing order of influence), simulated the model and then compared it with the linearly predicted result. The individual results are shown in Figure 3.13. In Figure 3.12 we summarize the results with a series of box plots, each one representing the errors committed over the first 9 modes, depending on the considered number of parameters.

For the first 5 parameters (up until h_c) we can see that the average error over the first 9 modes is always very close to zero. The first modal frequency appears as an outlier for 4 or more parameters, after including the variation of $h_{f,1}$. This study alone is not

sufficient to determine exactly which parameters interact non-linearly with $h_{f,1}$. However, we can notice that the first modal frequency is also the one presenting the greatest error in the study of the combined effect of all fan braces in Figure 3.11, and in both cases this modal frequency is similarly overestimated. Thus it seems reasonable to think that this happens because of the interaction between the two fan brace parameters, $h_{f,2}$ and $h_{f,1}$. This also seems justified if we consider that increasing a brace height has the effect of locally stiffening the plate. Since these two bars lie next to each other, it is likely that the added stiffness obtained by increasing both heights is not significantly higher than the one obtained by only altering one of them. However, this doesn't explain why a similarly high error is not observed for mode 4, where the modal shape of the top plate is the same.

Finally, a highly non-linear behaviour is observed when including the last parameter, x_{W}. Here the frequencies of the simulated model are significantly lower than those predicted, especially for mode 5. Since the only other parameter among those considered which caused a lowering of the frequencies was x_{LB2}, as seen in Figure 3.7, this suggests that this large decrease could be due to the combined effect of x_{W} and x_{LB2}. It is also noteworthy that, as seen in Figure 3.7, the influence of x_{W} alone on the eigenfrequency of mode 5 was actually found to be minimal. This non-linear and more complex behavior could also be caused by the aforementioned change in the soundbox air volume, which occurs every time we modify the outline shape.

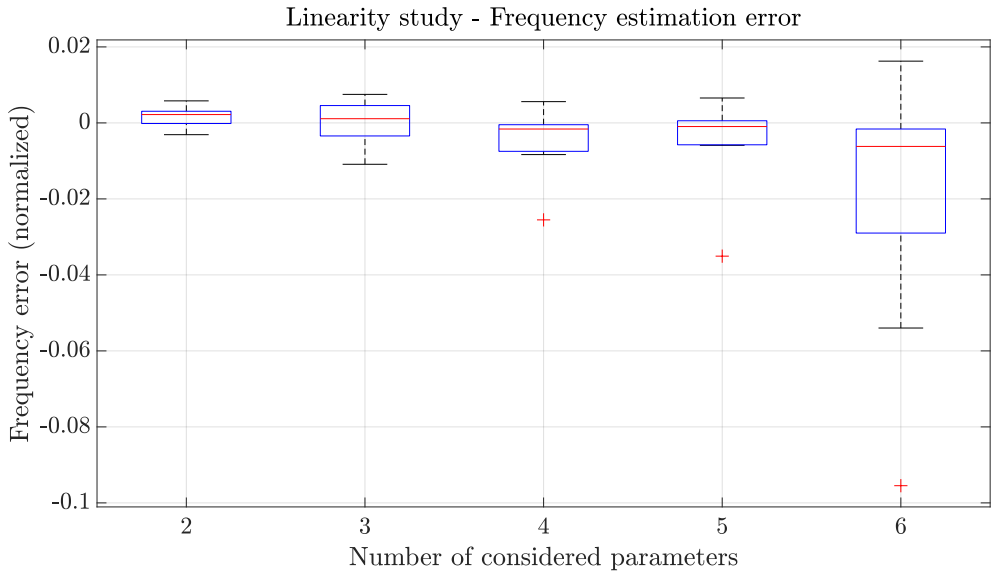

Figure 3.12: Box plots for the errors committed over the first 9 modes by using the linear approximation, for an increasing number of considered parameters.

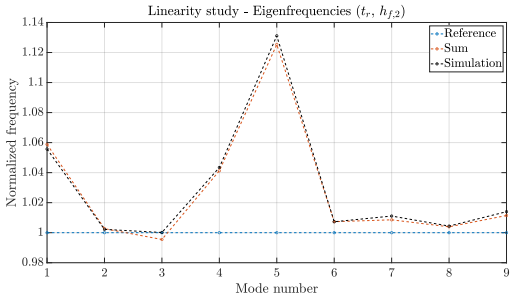

(a) First 2 parameters.

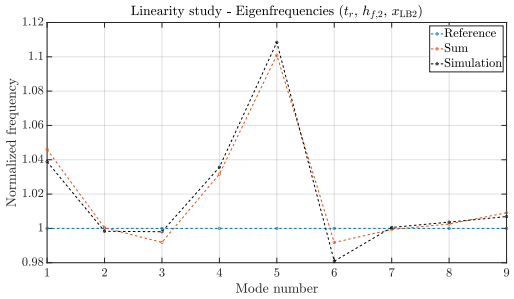

(b) First 3 parameters.

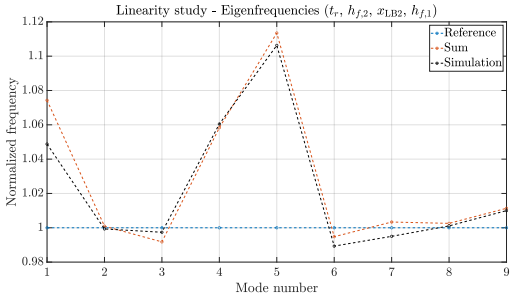

(c) First 4 parameters.

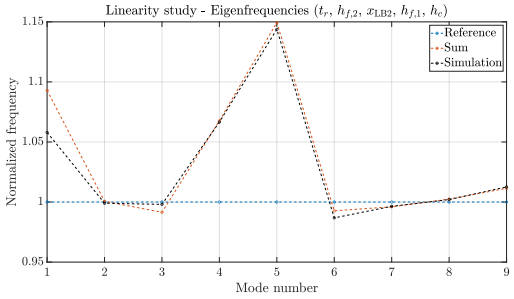

(d) First 5 parameters.

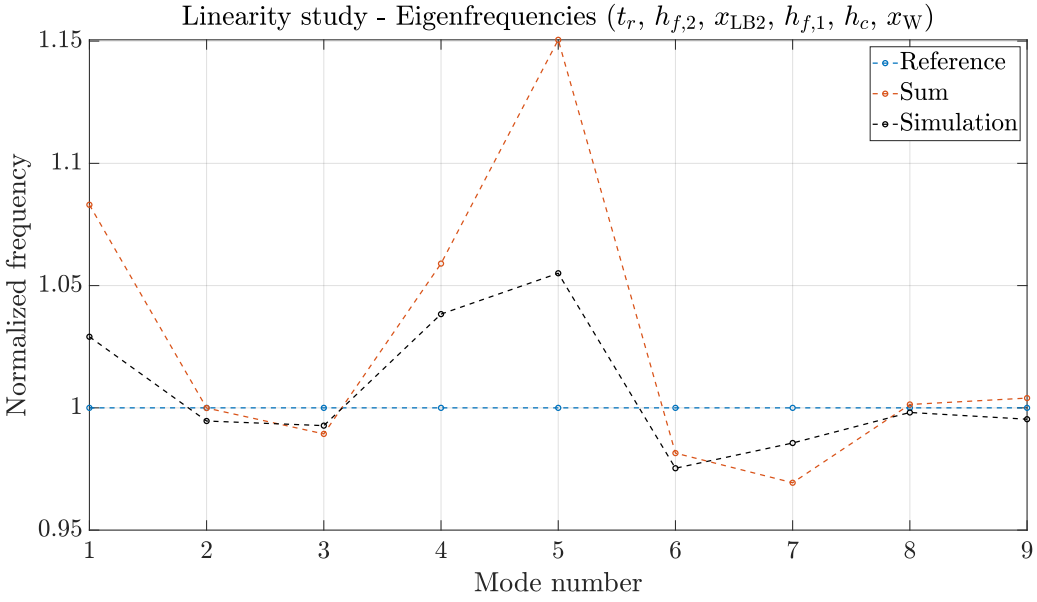

(e) First 6 parameters.

Figure 3.13: Relative frequency variations obtained by simulating models with multiple parameter changes, compared with the ideal linear results. Each time a new parameter is considered, based on its influence on the guitar eigenfrequencies.

3.4. Frequency Response

In this section we analyze the frequency response of the guitar by means of its bridge mobility and measured SPL. The load is modeled as a harmonic force perpendicular to the soundboard, distributed on a circular area of 2 mm radius at the contact between the bridge and the top surface. The position of the load is also shifted towards one end of the bridge (which we consider the "treble side", although the model is symmetric) to avoid suppression of modes with nodal lines running across the center of the soundboard.

Furthermore, for this study we also model the structural damping in the form of Rayleigh damping. The stiffness damping parameter is set to $\beta = 2 \times 10^{-6}$ s, while no mass damping term is considered, following a commonly employed approach [1, 2, 18].

The velocity is measured as the surface average of the component of the plate velocity in the same direction of the force, taken over the area where the load was applied. The driving point mobility is thus obtained as the absolute value of the ratio between the velocity and the applied force. The SPL is measured at a point placed 20 cm above the center of the soundboard.

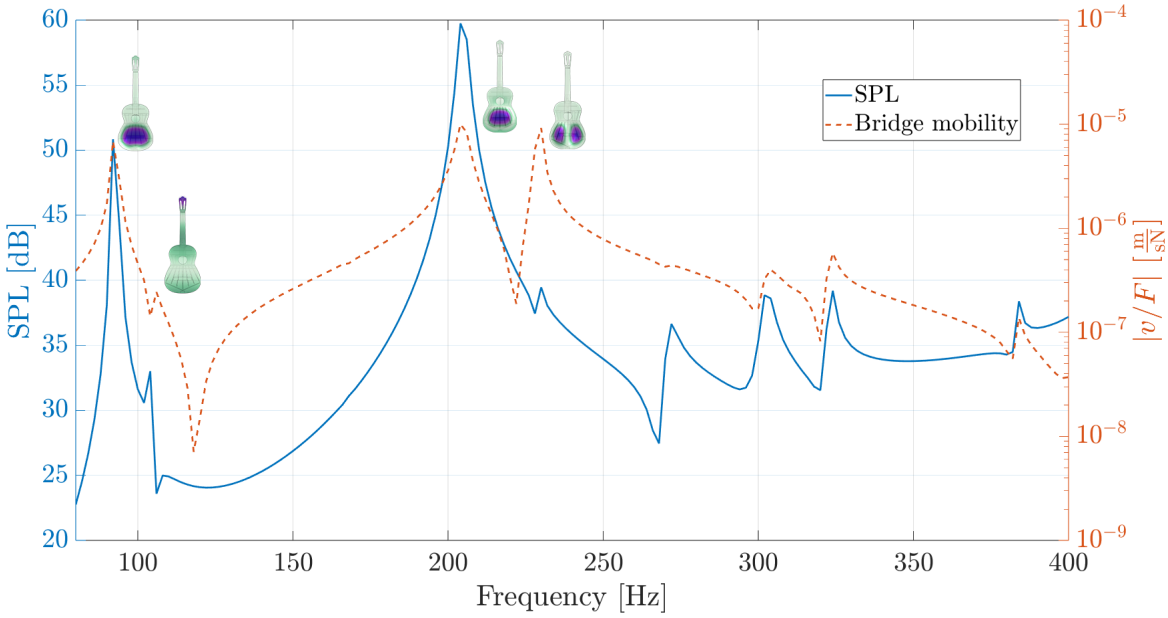

Figure 3.14: SPL as a function of frequency, compared with the driving-point bridge mobility, measured on the base guitar model. For the first 4 peaks the insets represent the corresponding mode shapes.

In Figure 3.14 we plot and compare the two quantities as functions of the driving frequency. The two curves have similar peaks and minima, confirming that the bridge mobility is a good descriptor of the sound radiated by the instrument. As expected, the strongest peaks correspond to mode 1 and mode 4, due to their monopolar shape and significant internal volume change. While one might anticipate mode 1 to exhibit stronger radiation than mode 4 due to its breathing motion, the opposite is observed. However, this behaviour is not unprecedented, as several findings in the literature support mode 4 as the most efficient sound radiator in the low-frequency range [5, 6, 33].

Mode 2 corresponds to a lesser peak in the mobility but still contributes slightly to the sound radiation, as it involves some bending of the soundboard too. Mode 5 presents a strong peak in the bridge mobility but a much weaker one in the SPL; this is due to its dipole shape, which is inefficient at radiating sound at low frequencies. Mode 3, which is purely a neck-bending mode, seems to have no effect on either mobility or SPL, confirming that modes of this type are practically irrelevant for sound radiation. Since modes 6 and 7 mostly involve back motion, and we are only measuring the sound pressure in front of the top plate, there is no clear peak in the SPL associated with them. Similarly there is also no corresponding peak in the mobility, due to its measurement location.

It must be noted that the measurement location of the SPL also plays a major role for the top plate-dominated modes, especially those with more complex shapes. In particular, the SPL peak of mode 5 is diminished by the fact that the evaluation point is aligned with a minimum of its radiation pattern. This is illustrated in Figure 3.15, where we show the radiation patterns for frequencies close to the three most relevant modes (mode 1, 4 and 5). The 2D plots depict the SPL measured on a circle of 20 cm radius in the plane orthogonal to the soundboard, passing through the point where the frequency response was evaluated (corresponding to angle 0°). The 3D radiation patterns, instead, represent the SPL measured on the surface of the air sphere. The characteristic dipole radiation of mode 5 is clearly visible, while mode 4 exhibits a cardioid pattern. A similar pattern is found for mode 1, though in this case the back motion is larger and gives rise to a back lobe, which becomes more pronounced for lower frequencies.

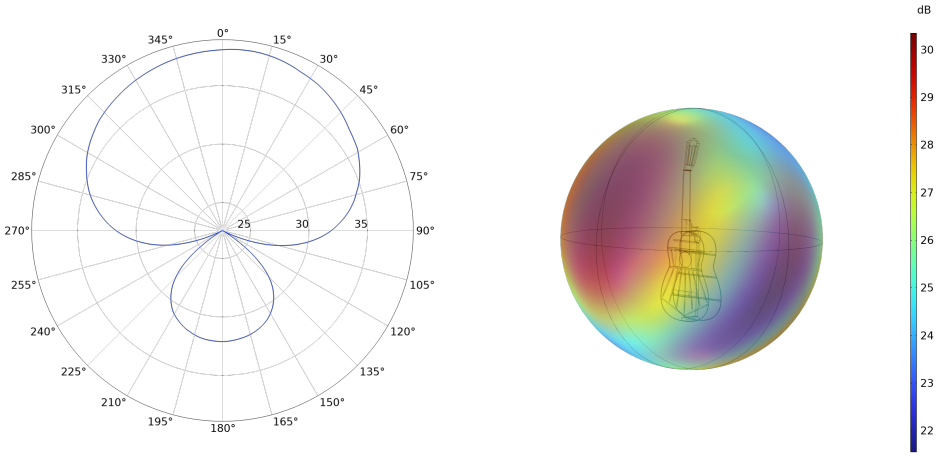

(a) Driving frequency: 90 Hz (around mode 1)

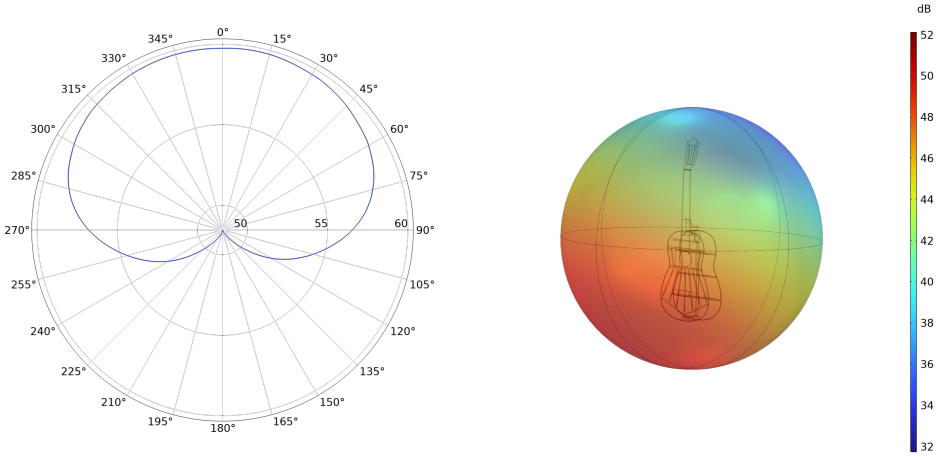

(b) Driving frequency: 204 Hz (around mode 4)

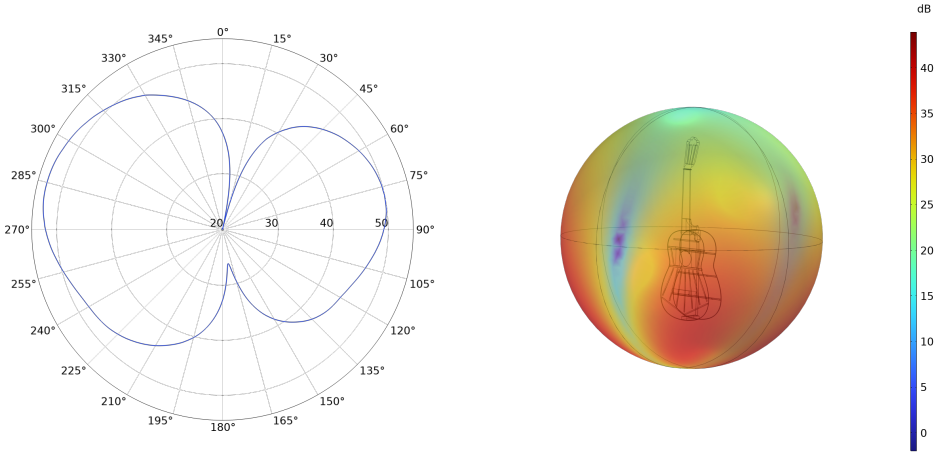

(c) Driving frequency: 228 Hz (around mode 5)

Figure 3.15: Radiation patterns (SPL) measured for frequencies around three guitar modes, in a plane orthogonal to the soundboard (2D) and over the air sphere surface (3D). A 0° angle corresponds to being exactly in front of the soundboard.

In Figure 3.16 we show the SPL across a few models when applying either changes to the bracing or the outline shape. As a simple way to compare the overall sound radiation performance of the different models, we compute the total SPL summed across the 80-400 Hz frequency range. The relative variations of this quantity, with respect to the reference model, are shown in Table 3.2.

Figure 3.16a shows the reference SPL against that of two models selected because of their significant eigenfrequency variation, as seen in Section 3.3. The shift in the frequency peaks is consistent with the change observed in the corresponding eigenfrequencies. Increasing the height of the braces mostly affects the frequency of mode 1, 4 and 5, while not significantly impacting the sound level. This suggests that we can alter this feature to control the timbre of the instrument without influencing its ability to radiate sound.

Widening the outline, instead, has a more significant impact on the frequency response. The first two modes seem to radiate less efficiently, while the situation is reversed when going above the frequency of mode 4.

Figure 3.16b shows the resulting SPL when removing the two bars in the upper bout, whose effect on the eigenfrequencies was already found to be minimal. The frequency responses of the two modified models mostly match the reference one, both in peaks location and amplitude. This further strengthens the argument that these bars do not play a significant in role in either shaping the instrument timbre, or improving its radiation efficiency. At least in the 80-300 Hz frequency range, it is possible that the observed differences with respect to the base model fall within the uncertainty window of current modal testing techniques, therefore rendering the instruments virtually equivalent in this range from a measurement perspective [35].

Table 3.2: Relative variations of total SPL (%) compared to the reference model.

Model	**Relative Variation (%)**
Increased fan bar heights	$-0.733\,\%$
Wider outline	$1.888\,\%$
No t bar	$-0.47\,\%$
No ht bar	$0.21\,\%$

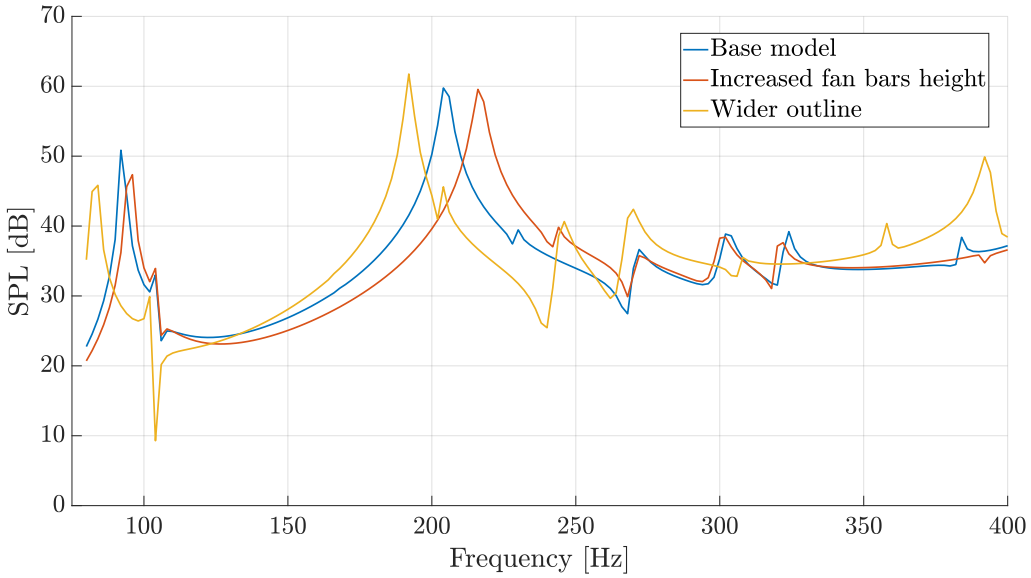

(a) SPL comparison for models with changes in outline shape or bracing height.

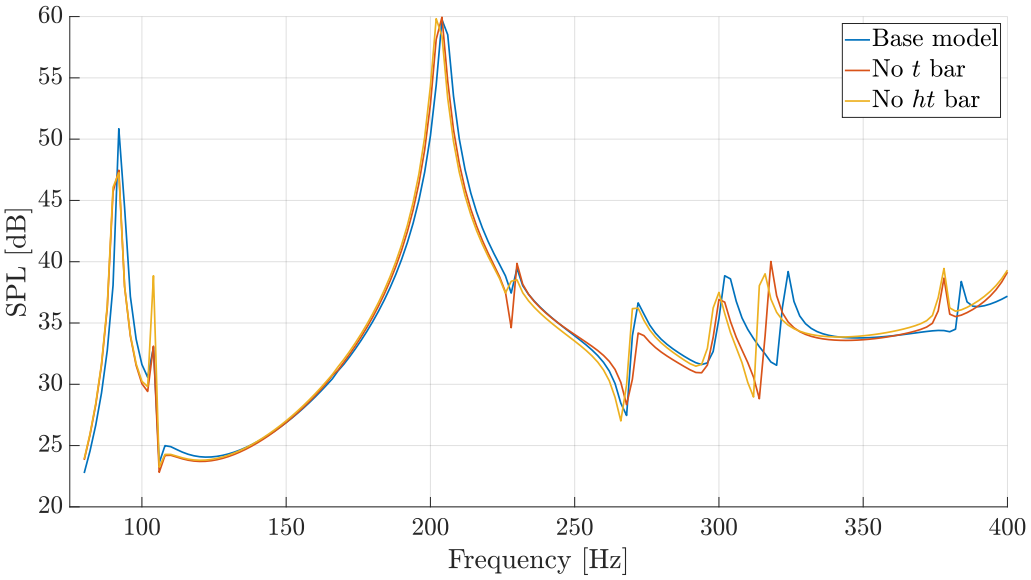

(b) SPL comparison for models devoid of upper bout braces.

Figure 3.16: SPL as a function of frequency compared across models with different geometry or bracing.

4 | Conclusions and Future Works

For this thesis we developed and described a parametric and native CAD guitar model inspired by a historical design by Antonio de Torres, which presents many of the traditional elements of classical guitars. We successfully parameterized some of the most important features which are typically altered by guitar makers during the construction process, such as the shape of the bracing bars or the body outline.

By modifying these parameters, different geometries can be easily generated and exported for use in numerical simulation tools, where the vibrational and acoustic properties of the instrument can be studied.

In particular, by applying the Finite Element Method, we showcased the capabilities of this model and obtained some novel results. The air surrounding the entire instrument was also considered in the simulation, an important aspect that has often been overlooked in recent research.

Firstly, we performed a modal analysis of the instrument while varying, one at a time, some of its geometrical features. Focusing on the lower modes of vibration, we determined which of these features had a higher impact on the eigenfrequencies when modified. We then estimated how linearly the eigenfrequencies behave when multiple parameters are altered at the same time. First this was done for the fan brace heights, which showed an approximately linear behaviour. Then the same was done for the 6 most influential parameters, showing a quite close approximation for the first 5 parameters but a highly non-linear behaviour when including the last one. We assumed this was due to the non-linear interaction between the parameters which control the outline shape.

Since modifications to braces height in the upper bout and waist area had the least impact, we then tried to remove them and recompute the eigenfrequencies. The results on the upper bout braces showed that these bars do not play a significant role in determining the dynamic behaviour of the instrument. Coupled with the findings in [30], which show a similarly negligible effect on the static behaviour, this highlights that these bars may have persisted in the guitar design until now due to long-standing tradition rather than actual functionality. This result holds significant importance as, to the best of our

knowledge, it represents one of the first instances where numerical simulations provide valuable operational insights to luthiers regarding instrument design.

Lastly, we studied the instrument frequency response, by applying a harmonic load and measuring its bridge mobility and the sound radiated in front of the soundboard as a function of frequency. The results where consistent with the previous eigenfrequency studies, and confirmed that mode 1 and 4 (the two monopolar modes of the top and back plate) are the main contributors to sound radiation in the low frequency range, while the neck modes are practically irrelevant. To some extent, these findings justify the prior research focus on the guitar body alone when investigating the instrument's acoustic behaviour [18].

We also compared the frequency response across a few different guitar models. In particular, we further tested the two models without the upper bracing and showed that, also in terms of sound radiation, there was no significant variation with respect to the base model.

4.1. Future Works and Applications

Through the creation and detailed description of this parametric model, we plan to facilitate and streamline future research into the physics of guitars. Since the model was developed natively inside Fusion 360®, using its parameter functionality, this makes the customization accessible even for unexperienced users. Furthermore, the models can be readily translated into physical prototypes through the use of CNC routers or 3D printers. This can simplify the process of experimental validation, which also represents one possible direction to build upon the results of our work.

Due to practical limitations, only some of the controllable parameters were actually explored. Future research endeavors could use this model to focus on the effects of varying other features, like the width of the braces or the angle of the fan struts. One interesting prospect is the possibility of reproducing and simulating different common guitar shapes by manipulating the control point parameters, and even interpolate the shape across different models.

It is important to acknowledge that our model is based on a single specific design and, while the available parameters offer ample exploration possibilities, certain guitar models with radically different designs cannot be achieved without further modifications. Future works could involve creating new versions of our parametric model to address this limitation, for example to support asymmetric or steel-string guitars bracing patterns

(*X-bracing*). X-bracing patterns were explored in [36], though only the soundboard of the guitar was considered and the numerical model did not take into account the effect of air, which we could easily include in future research with our model. Even further, more modern and innovative designs can be studied, such as those employing mechanical metamaterials and lattice patterns to control the instrument sound, as seen in [1, 2]. In all these cases, our modular approach, which allows easy combination and removal of individual components, makes switching between these designs a simpler task.

Additionally, only a limited number of models were generated for the considered parameters. By appropriately sampling the parameter space, or just a subspace of it, subsequent studies can perform more detailed analyses or even build predictive models. In fact, the results obtained from FEM analysis on these parametric models can further serve as datasets for applying machine learning techniques, which allow the construction of comprehensive predictive models capable of returning various quantities of interest (such as eigenfrequencies or frequency response) for any given set of parameter values. For instance, Gonzalez et al. applied neural networks to predict the eigenfrequencies of a violin top plate [37] and then to run a parametric optimization process [38]. Badiane et al. also utilized machine learning methods to predict the frequency response of wooden plates from their mechanical parameters [39]. More recently, a similar approach was employed by Longo et al. to forecast the acoustic properties of an archtop guitar [18]. One of the ultimate aims of developing these predictive models is to make these technologies accessible to instrument makers and other users outside of the research field, who may lack the resources required to conduct numerical simulations. In this sense, machine learning provides a valuable tool for the democratization of research results, and a way to see those results finally employed in everyday practice. With our contribution, we aim to take a significant step towards achieving this goal.

Furthermore, the results obtained in this manner can not only assist instrument makers but also aid in the development of physics-based sound synthesis algorithms, where the output depends directly on the geometrical and material parameters of the modelled instrument. In this way the optimization process can be directly guided by assessing the final synthesised sound, as opposed to relying on features whose correlation with the actual instrument quality may not always be clear. An early step in this direction can be found in [40].

At the time of writing, our model is already being employed in other studies, which will hopefully aid in further demystifying the art and science of guitar making.

Bibliography

[1] Mattia Lercari. A numerical study on mechanical metamaterials in classical guitars. Master's thesis, Politecnico Di Milano, 2022. Available at https://hdl.handle.net/10589/190000.

[2] Mattia Lercari, Sebastian Gonzalez, Carolina Espinoza, Giacomo Longo, Fabio Antonacci, and Augusto Sarti. Using mechanical metamaterials in guitar top plates: A numerical study. *Applied Sciences*, 12(17), 2022. ISSN 2076-3417. doi: 10.3390/app12178619. URL https://www.mdpi.com/2076-3417/12/17/8619.

[3] I. Sloane. *Classic Guitar Construction: Diagrams, Photographs, and Step-by-step Instructions*. E.P. Dutton, 1966. ISBN 9780525082002. URL https://books.google.it/books?id=r4g8XwAACAAJ.

[4] E. V. Jansson. A study of acoustical and hologram interferometric measurements of the top plate vibrations of a guitar. *Acta Acustica united with Acustica*, 25(2): 95–100, 1971. ISSN 1610-1928. URL https://www.ingentaconnect.com/content/dav/aaua/1971/00000025/00000002/art00007.

[5] Ian M. Firth. Physics of the guitar at the Helmholtz and first top-plate resonances. *The Journal of the Acoustical Society of America*, 61(2):588–593, 02 1977. ISSN 0001-4966. doi: 10.1121/1.381302. URL https://doi.org/10.1121/1.381302.

[6] N.H. Fletcher and T. Rossing. *The Physics of Musical Instruments*. Springer New York, 2008. ISBN 9780387983745. URL https://books.google.it/books?id=9CRSRYQlRLkC.

[7] George Norman Jenner. *Computer aided design of acoustic guitars*. PhD thesis, UNSW Sydney, 1986.

[8] Evaggelos Kaselouris, Makis Bakarezos, Michael Tatarakis, Nektarios A Papadogiannis, and Vasilis Dimitriou. A review of finite element studies in string musical instruments. In *Acoustics*, volume 4, pages 183–202. MDPI, 2022.

[9] Alexander Brauchler, Sebastian Gonzalez, Manuel Vierneisel, Pascal Ziegler, Fabio

Antonacci, Augusto Sarti, and Peter Eberhard. Model-predicted geometry variations to compensate material variability in the design of classical guitars. *Scientific Reports*, 13, 08 2023. doi: 10.1038/s41598-023-37943-y.

[10] Mattia Vassena. Modal analysis of classical guitar soundboard with parametric shape and fan bracing. Master's thesis, Politecnico Di Milano, 2021. Available at `https://hdl.handle.net/10589/177453`.

[11] Davide Salvi, Sebastian Gonzalez, Fabio Antonacci, and Augusto Sarti. Modal analysis of free archtop guitar top plates. *The Journal of the Acoustical Society of America*, 150(2):1505–1513, 08 2021. ISSN 0001-4966. doi: 10.1121/10.0005937. URL `https://doi.org/10.1121/10.0005937`.

[12] Sebastian Gonzalez, Davide Salvi, Fabio Antonacci, and Augusto Sarti. Eigenfrequency optimisation of free violin plates. *The Journal of the Acoustical Society of America*, 149(3):1400–1410, 03 2021. ISSN 0001-4966. doi: 10.1121/10.0003599. URL `https://doi.org/10.1121/10.0003599`.

[13] Laura Lodetti, Sebastian Gonzalez, Fabio Antonacci, and Augusto Sarti. Stiffening cello bridges with design. *Applied Sciences*, 13(2), 2023. ISSN 2076-3417. doi: 10.3390/app13020928. URL `https://www.mdpi.com/2076-3417/13/2/928`.

[14] Alexander Brauchler, Pascal Ziegler, and Peter Eberhard. Numerical Models for Classical Guitars with Updated Parameters from Experimental Data. In *Forum Acusticum*, pages 2155–2161, Lyon, France, December 2020. doi: 10.48465/fa.2020.0072. URL `https://hal.science/hal-03235385`.

[15] A. Ezcurra, M.J. Elejabarrieta, and C. Santamaría. Fluid–structure coupling in the guitar box: numerical and experimental comparative study. *Applied Acoustics*, 66(4):411–425, 2005. ISSN 0003-682X. doi: https://doi.org/10.1016/j.apacoust.2004.07.010. URL `https://www.sciencedirect.com/science/article/pii/S0003682X04001240`.

[16] María Elejabarrieta, A. Ezcurra, and Carlos Santamaria. Coupled modes of the resonance box of the guitar. *The Journal of the Acoustical Society of America*, 111:2283–92, 06 2002. doi: 10.1121/1.1470163.

[17] Ove Christensen and Bo B. Vistisen. Simple model for low-frequency guitar function. *The Journal of the Acoustical Society of America*, 68(3):758–766, 09 1980. ISSN 0001-4966. doi: 10.1121/1.384814. URL `https://doi.org/10.1121/1.384814`.

[18] Giacomo Longo, Sebastian Gonzalez, Fabio Antonacci, and Augusto Sarti. Pre-

dicting the acoustics of archtop guitars using an ai-based algorithm trained on fem simulations. 09 2023. doi: 10.61782/fa.2023.0662.

[19] Henna Tahvanainen. *Modelling body vibration and sound radiation of a modified kantele*. PhD thesis, 11 2012.

[20] W.S. Slaughter. *The Linearized Theory of Elasticity*. Birkhäuser Boston, 2002. ISBN 9780817641177. URL https://books.google.it/books?id=jUzdtBNAPa4C.

[21] COMSOL. *Structural Mechanics Module User's Guide*. COMSOL, 2024. URL https://doc.comsol.com/5.4/doc/com.comsol.help.sme/StructuralMechanicsModuleUsersGuide.pdf. Accessed on March 13, 2024.

[22] Martino Quintavalla, Federico Gabrielli, and Claudio Canevari. Grading materials for stringed instruments soundboards: An approach considering the orthotropic elastic and damping properties. *Applied Acoustics*, 187:108521, 2022. ISSN 0003-682X. doi: https://doi.org/10.1016/j.apacoust.2021.108521. URL https://www.sciencedirect.com/science/article/pii/S0003682X21006150.

[23] Frédéric Nataf. Absorbing boundary conditions and perfectly matched layers in wave propagation problems. In *Direct and Inverse problems in Wave Propagation and Applications*, volume 14 of *Radon Ser. Comput. Appl. Math.*, pages 219–231. de Gruyter, 2013. URL https://hal.science/hal-00799759.

[24] Alvin Bayliss, Max Gunzburger, and Eli Turkel. Boundary conditions for the numerical solution of elliptic equations in exterior regions. *Siam Journal on Applied Mathematics - SIAMAM*, 42, 04 1982. doi: 10.1137/0142032.

[25] COMSOL. *Acoustics Module User's Guide*. COMSOL, 2024. URL https://doc.comsol.com/5.4/doc/com.comsol.help.aco/AcousticsModuleUsersGuide.pdf. Accessed on March 7, 2024.

[26] COMSOL. Detailed explanation of the finite element method, n.d. URL https://www.comsol.com/multiphysics/finite-element-method. Accessed on March 7, 2024.

[27] Hossein Mansour. Modal Analysis of the Setar: A Numerical–Experimental Comparison. *Journal of Vibration and Acoustics*, 137(6):061006, 12 2015. ISSN 1048-9002. doi: 10.1115/1.4030863. URL https://doi.org/10.1115/1.4030863.

[28] Özge Akar and Kai Willner. The modal behaviour of a violin corpus. *Journal of New Music Research*, 0(0):1–22, 2024. doi: 10.1080/09298215.2024.2321869. URL https://doi.org/10.1080/09298215.2024.2321869.

[29] R. Courtnall and A. Lucas. *Making Master Guitars*. Hale, 1993. ISBN 9780709048091. URL https://books.google.it/books?id=UqD-AQAACAAJ.

[30] Rebecca Superbo. The influence of scale length and string pre-stress in the vibrational and radiative properties of guitars. Master's thesis, Politecnico di Milano, 2024.

[31] Vintage Guitar. Antonio de torres (1863), n.d. URL https://www.vintageguitar.com/3434/antonio-de-torres-1863/. Accessed on February 22, 2024.

[32] Forest Products Laboratory. *Wood Handbook: Wood as an Engineering Material*. University Press of the Pacific, 2000. ISBN 9780898750829. URL https://books.google.it/books?id=YjHgPAAACAAJ.

[33] Bernard E Richardson. The acoustical development of the guitar. *Catgut Acoustical Society Journal*, 2(5):1–10, 1994.

[34] Miroslav Pastor, Michal Binda, and Tomáš Harčarik. Modal assurance criterion. *Procedia Engineering*, 48:543–548, 2012. ISSN 1877-7058. doi: https://doi.org/10.1016/j.proeng.2012.09.551. URL https://www.sciencedirect.com/science/article/pii/S1877705812046140. Modelling of Mechanical and Mechatronics Systems.

[35] Seth Lowery and Andrew Piacsek. A tool for quantifying the uncertainty measurements of violin impact response. volume 46, page 035003, 01 2022. doi: 10.1121/2.0001675.

[36] Y. Giro, J.-L. Le Carrou, A. Vincenti, S. Dartois, R. Viala, and B. Navarret. Predicting the effects of bracing pattern modifications on acoustic guitar soundboards. European Acoustics Association, January 2024. doi: 10.61782/fa.2023.0627. URL http://dx.doi.org/10.61782/fa.2023.0627.

[37] Sebastian Gonzalez, Davide Salvi, Daniel Baeza, Fabio Antonacci, and Augusto Sarti. A data-driven approach to violin making, 2021.

[38] Davide Salvi, Sebastian Gonzalez, Fabio Antonacci, and Augusto Sarti. Parametric optimization of violin top plates using machine learning. *CoRR*, abs/2102.07133, 2021. URL https://arxiv.org/abs/2102.07133.

[39] David Giuseppe Badiane, Raffaele Malvermi, Sebastian Gonzalez, Fabio Antonacci, and Augusto Sarti. On the prediction of the frequency response of a wooden plate from its mechanical parameters. In *ICASSP 2022 - 2022 IEEE International Conference on Acoustics, Speech and Signal Processing (ICASSP)*, pages 461–465, 2022. doi: 10.1109/ICASSP43922.2022.9746760.

[40] Sebastian Gonzalez, Mark Rau, Carolina Espinoza, Giacomo Longo, Fabio Antonacci, and Augusto Sarti. Sound synthesis of geometric and material changes in archtop guitars: towards the timbral design of musical instruments. 09 2023. doi: 10.13140/RG.2.2.19090.22724.

A | Appendix A

The CAD files (in STEP format) of the models used to run the simulations, along with the corresponding COMSOL project files (without results) can be retrieved at **Classical Guitar Modeling**.

The Fusion 360® parametric model can be obtained at **Fusion 360 Parametric model**.

List of Figures

List of Tables

Acknowledgements

I would like to express my gratitude towards my advisor, Fabio Antonacci, for giving me the opportunity to work on this deeply fascinating topic and encouraging me along my journey. I must also deeply thank my co-supervisor, Sebastian, whose continued help and valuable insight has been fundamental in achieving the results of this work, and for providing a good environment to work in.

A special thought goes to my girlfriend, Sara, whose love and unwavering support has carried me throughout all the biggest challenges during the last twelve years. This would have been impossible without you.

Lastly, I am grateful to my family for their tireless patience, understanding, and constant belief in me.